FACULTY OF MEDICINE AND HEALTH SCIENCES

Validation of personalized cartilage thickness mapping of the distal femur in a healthy population

Femke Dhooge
Student number: 01803953

Supervisor(s): Prof. Dr. Emmanuel Audenaert, Dr. Aline Van Oevelen

A dissertation submitted to Ghent University in partial fulfilment of the requirements for the degree of Master of Medicine in Medicine

Academic year: 2021 – 2023

GHENT UNIVERSITY

"The author and the promotor give the permission to use this thesis for consultation and to copy parts of it for personal use. Every other use is subject to the copyright laws, more specifically the source must be extensively specified when using results from this thesis."

Date 14 / 11 / 2022

(handtekening)

Name (student) Femke Dhoge

Emmanuel Audenaert (Authentication)

Digitaal ondertekend door Emmanuel Audenaert (Authentication)
Datum: 2022.11.14 12:21:25 +01'00'

(promotor)

Prologue

This master thesis is part of the ongoing doctoral research "Personalized cartilage prediction of the lower limb: Validation of soft tissue anatomy at the level of the knee in a control population" at the department of physical therapy and orthopaedics at University Hospital (UZ) Ghent. Ethical approval was obtained from the ethics committee of UZ Ghent (appendix A).

A sincere thanks to my co-supervisor Dr. Aline Van Oevelen for her meticulous follow-up, guidance, accessibility and support, to my supervisor Prof. Dr. Emmanuel Audenaert for his accessibility, revision and supervision and to co-student Ragna Weytens to write the "Introduction" and "Materials and methods" sections with me.

A heartfelt thank you to all the volunteers for their enthusiastic participation, to Shirley Vlieghe and Raynaud Vanwolleghem for customizing the images and to Anna-Maria Makri-Pistikou and Arjen Van de Walle for the final revisions.

Contents

List of figures

List of tables

List of abbreviations

UZ	University Hospital
OA	Osteoarthritis
MRI	Magnetic resonance imaging
3D	Three-dimensional
CT	Computed tomography
SSM	Statistical shape model
MCL	Medial collateral ligament
LCL	Lateral collateral ligament
ACL	Anterior cruciate ligament
PCL	Posterior cruciate ligament
ECM	Extracellular matrix
angle Q	Quadriceps angle
SD	Standard deviation
mm	Millimetre
2D	Two-dimensional
VAS-p	Visual analogue scale for pain
ms	Millisecond
cm	Centimetre
kg	Kilogram
RMSE	Root Mean Square Error
ASD	Average Surface Distance
HD	Hausdorff distance

Abstract

Introduction: Congruent, low-friction movement between the articulating surfaces of a synovial joint is a crucial prerequisite for sustained and efficient joint function. However, where disorders in joint formation or maintenance (homeostasis) occur, mechanical overloading and osteoarthritis (OA) will follow. OA is the most common chronic joint disease with a global prevalence of 7%. Knee OA constitutes 83% of the global disease burden for OA. The prevalence exacerbates over time and is expected to continue to increase due to ascending obesity and trends of an aging population. Counterintuitively, little is known about the ethology and causes of the onset and progression of the disease. As *in vivo* measurement of knee joint contact forces remains challenging, computational musculoskeletal modelling becomes more popular for non-invasive estimation of joint loading distribution. Typically these methods depend on cumbersome and time-consuming manual segmentation of joint geometry. The current study aims to validate an automated method for personalized distal femoral cartilage mapping developed within the department of orthopaedics at Ghent University Hospital (UZ).

Materials and methods: A total of 30 subjects were included in the current validation study. They underwent a kinetic study and magnetic resonance imaging (MRI) of the lower extremities. A three-dimensional image (3D) of the distal femur, proximal tibia and right distal femoral cartilage was generated by manual segmentation. The femur, required for the cartilage mapping, was reconstructed by a statistic shape model (SSM). Cartilage geometry prediction using a node-specific thickness map was compared with manual segmentation.

Results: The validation study of automated distal femoral cartilage mapping resulted in a median Root Mean Square Error (RMSE) (0.6723 mm), Average Surface Distance (ASD) (0.5580 mm) and Hausdorff Distance (HD) (2.4165 mm) with their corresponding range. Visual illustration of site-specific anomalies describes the regions of greatest error.

Discussion: The error relative to the local cartilage thickness is a tolerable deviation. The median HD indicates that further optimisation of the method is warranted. Despite the high HD values, the average error is relatively low. Thus, there is a large distribution in the accuracy of prediction in a subject. The range of the RMSE, ASD and HD indicates a large interpersonal variation. The main prediction error is located frontally, proximally and bilaterally on the femoral trochlea and distally at the location where the medial and lateral condylar cartilage meet. These error rates should not just be attributed to the prediction model.

Conclusion: SSM can detect anatomic and biomechanical risk factors more efficiently by replacing cumbersome and operator-dependent manual segmentation. Estimating joint forces on the knee and soft tissue function in the knee and predicting secondary kinematics of the knee will be possible and patient-specific joint preservation or replacement surgery of the knee will be applicable using a prediction model. Despite optimisation of the cartilage mapping model being further warranted, the validation study yielded hopeful results.

Dutch version (appendix B).

Introduction

1. Statement of Problem

OA is the most common chronic joint disease with a global prevalence of 7% (1, 2). Among people over 60 years old, it affects about 10% of men and 18% of women (3). The prevalence exacerbates over time and is expected to continue to increase due to ascending obesity and trends of an aging population (4). Of the global burden of OA, the knee constitutes 83% with a population prevalence of 3.64% (5). In addition to these alarming rates, OA represents a major socioeconomic impact (3, 6, 7). Counterintuitively, with such a high impact of knee OA, little is known about the ethology and causes of the incident and progression of this disease. In part, this explains why curative drugs do not exist (6, 8).

Computational models, supportive methods in the clinical decision-making process, are being developed and investigated to indirectly estimate joint forces on the knee and soft tissue function in the knee and predict secondary kinematics of the knee. These *in silico* techniques rely on accurate anatomical information about the architecture of the musculoskeletal system, which is usually obtained by manual segmentation of computed tomography (CT) and/or MRI images. Theoretically, these non-invasive models would be conducive to optimise patient-specific treatment. This may belittle the limitations of current treatment based on subjective, static and mostly qualitative assessment (9, 10). Practical implementation is hampered by the costly and infrequently available MRI image acquisition. Additionally, the crucial manual segmentation of the musculoskeletal anatomical structures is time-consuming and labour-intensive and produces human operator-dependent bias. This creates the need to develop an automatic model that can predict the anatomy of soft tissue and bone in the knee (11, 12).

The aforementioned obstacles can be overcome by musculoskeletal prediction methods with static shape analysis (13). Thus, Audenaert et al. developed a validated method to fully and automatically segment the lower limbs by CT (14). Subsequently, personalized cartilage prediction was designed through cartilage thickness maps by Van Houcke et al. (Materials and methods – 5.) (13). Based on this, one obtains an anatomical cartilage model in a more time-efficient and non-operator-dependent manner. Audenaert et al. additionally developed methods using discrete element rigid body spring models based on geometric morphometry to predict the course, origin and insertion of muscles and tendons (15, 16). Peiffer et al. described the mapping of bone, cartilage and soft tissue for the ankle joint relying on previously mentioned studies (13, 16, 17). Regarding the knee, Van Dijck et al. developed a SSM to predict the geometry of the tibiofemoral cartilage relying on 524 MRIs (18). SSMs accurately describe dense shape representations and their variations in a population sample. A plausible,

patient-specific prediction can be effected using a minimal number of variables. A normal variant can be qualitatively and quantitatively distinguished from outlier shape entries or clinical abnormalities. SSM already finds multiple applications in individualised clinical settings, such as image segmentation or treatment determination based on an expected prognosis (19). A well know patient-specific tool by accurately imaging the anatomy involves total knee arthroplasty. This results in a more accurate alignment of an implant, a time-saving operation and a better subjective outcome for the patient. All this ensures a lower cost (20, 21).

The purpose of the current study is to enable patient-specific prediction of the cartilage layer geometry of the distal femur and validation of this cartilage mapping. Hereto a novel methodological workflow previously developed within the department of orthopaedics at UZ Ghent is validated. The goal of the longer-term study, of which this study is a part, is to develop a personalized generic computational model for the entire musculoskeletal and soft tissue anatomy of the knee.

2. Anatomy of the knee

2.1. Knee joint

The knee is a synovial joint that includes the tibiofemoral joint and the patellofemoral joint. The bony joint structures are the distal end of the femur, the proximal tibial epiphysis and the patella. A thick layer of hyaline cartilage covers all previous joint surfaces (figure 1) (22-24).

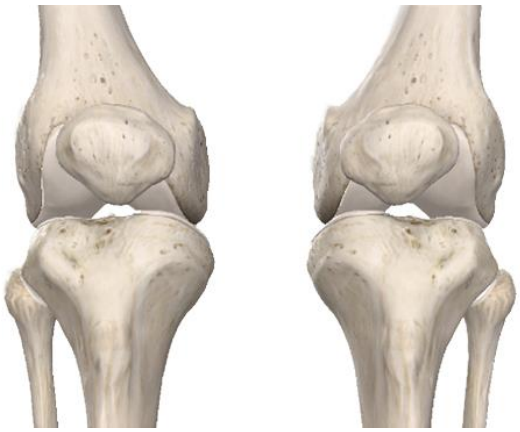

Figure 1: The frontal coronary view of the knee's bony anatomy and cartilaginous structure. The anterior cartilage layer on the femur is the paler volume on the darker underlying bone structure (25).

2.2. Bone anatomy of the knee

2.2.1. Femur

The medial and lateral femoral condyles articulate correspondingly with the medial and lateral tibial plateau. Both femoral condyles are convex in the coronal and sagittal plane with a stronger arch dorsally. The lateral condyle has a larger radius in the coronal plane. In the axial plane, the radius of the medial femoral condyle is about 3 mm larger (23, 24, 26).

The trochlea covers the anterior surface of the distal femur. The approximately 5.2 mm deep trochlear groove splits the trochlea into a medial and lateral facet complementary to the patellar joint surface (27). The lateral facet is larger than the medial and extends further proximally. The femoral notch is the continuation of the trochlear groove, which distally deepens and extends laterally. The facets merge distally into the medial and lateral femoral condyles (figure 2) (27, 28).

(a) *(b)*

Figure 2: Anterior (a) and posterior (b) coronary view of the left distal femoral epiphysis (25).

2.2.2. Tibia

The proximal tibial plateau consists of two condyles separated by a median intercondylar eminence. Despite the almost flat appearance of the condyles, the medial tibial plateau is slightly biconcave, while the lateral plateau is slightly convex in the sagittal plane and concave in the coronal plane (figure 3) (23, 24, 29).

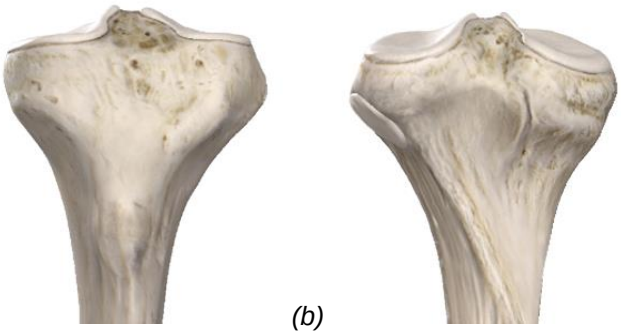

(a) *(b)*

Figure 3: Anterior (a) and posterior (b) view of the left proximal tibial epiphysis (25).

2.2.3. Patella

The patella is the largest sesamoid bone in the body (22). The anterior surface of the patella is convex (27). The posterior surface includes the articular side, articulating with the femoral trochlea (figure 4). The articulation side has a total of 7 facets. The entire surface is divided into medial and lateral facets by a median longitudinal ridge. The lateral is wider to be complementary to the femoral facets. Nevertheless, the articular surfaces of the patella and femoral are not completely congruent (22-24, 27). Only the upper two-thirds of the patella is used as the interface. The cartilage layer posterior to the patella is the thickest cartilage layer found in the body, which is 7 mm (27).

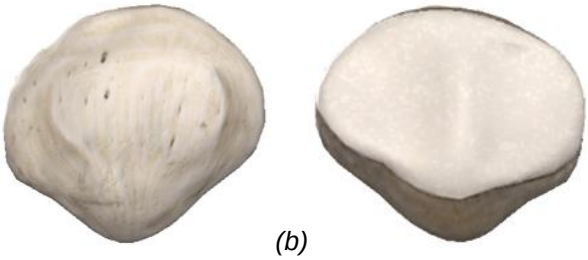

(a) *(b)*

Figure 4: Anterior (a) and posterior (b) view of the left patella (25).

2.3. Cartilage

2.3.1. Composition

Articular cartilage, usually hyaline cartilage, is a load-bearing layer of extracellular matrix (ECM) with special viscoelastic characteristics. This specialized connective tissue layer is porous, low in permeability and hydrated with type II collagen and proteoglycan as the dominant structural components (30, 31). The concentrations and gradients of these constituents vary with depth and location. This results in depth-dependent properties, directional differences in tissue tension and inhomogeneous local tissue deformation and tension. In superficial layers, the collagen network is densest and oriented approximately tangentially to the articular surface. In the deeper cartilage layers, collagen fibres run perpendicular to the joint surface and the content of proteoglycans is highest. The deepest layer is calcified (30-34). Production of this porous structure is accomplished by chondrocytes. This production depends on the number of cells present which decreases with age (35). Chondrocytes are specialized mesenchymal cells that occupy only 2% of total cartilage volume (30).

2.3.2. Cartilage thickness, distribution and measurement method

Incongruent joints, such as the knee, contain a thick layer of cartilage. Forces on the knee joint affect this thickness. Gender, age, weight and height help determine these acting forces. For instance, women have thinner cartilage than men and the quality of cartilage decreases with age. Cartilage is thicker and the cartilage surface more extensive in tall and heavy individuals. Cartilage thickness in the joint is additionally site-dependent. The cartilage layer is thicker in the medial compartment and at points of cartilage-to-cartilage contact (36-40).

There are several methods to measure cartilage thickness in the knee (table 1). A primary non-invasive method is MRI measurement after constructing a 3D model (39, 41). Partial volume averaging reduces the sensitivity of this method by masking early chondral lesions such as fissures and cartilage flaps (42). An alternative method is based on arthrograms with standard double-contrast techniques. An arthrogram is a series of images, usually taken via fluoroscopy or MRI, of a joint after contrast injection. Roentgenographic magnification and invasiveness are disadvantages of this technique (36). Swann and Seedhom is a destructive needle probe technique in which a device with a sharp needle can pierce the cartilage surface and migrate through the cartilage. Only a cartilage fragment is preloaded because the subchondral bone is impossible to pierce. This measurement of the thickness of cartilage plugs or slices can only be effected post-mortem (37, 43, 44). A non-destructive technique such as ultrasound is inaccurate. A limitation of ultrasound is that a constant speed of sound must be assumed, whereas it can vary greatly between cartilage specimens (43, 44).

Table 1: Cartilage thickness based on literature.

Author	**Study population**	**Technique**	**Medial femoral condyle - mean (SD) mm**	**Lateral femoral condyle - mean (SD) mm**	**Medial tibial plateau - mean (SD) mm**	**Lateral tibial plateau - mean (SD) mm**
Li et al. (39)	6 healthy volunteers with an averaging 27 years	1,5T MRI-scan and the knee in 0° flexion - 3D models	I: 2.8 (0.3) C: 2.0 (0.4) O: 2.0 (0.4)	I: 1.7 (0.3) C: 2.0 (0.7) O: 2.1 (0.5)	<u>Anterior</u> I: 1.9 (0.5) C: 2.0 (0.6) O: 1.8 (0.5) <u>Central</u> I: 3.3 (0.4) C: 2.5 (0.6) O: 2.0 (0.6) <u>Posterior</u> I:2.0 (0.3) C:1.8 (0.3) O: 1.6 (0.4)	<u>Anterior</u> I:2.1 (0.6) C:2.0 (0.6) O: 1.4 (0.4) <u>Central</u> I:4.0 (0.9) C:3.2 (0.7) O: 2.0 (0.4) <u>Posterior</u> I:3.1 (0.5) C:2.8 (0.9) O: 1.8 (0.3)

Cohen et al. (41)	6 fresh-frozen cadaver knees averaging 50 years and 4 volunteers averaging 26 years	1,5T MRI-scan and the knee in approximately 0–20° flexion - 3D models	2,14 (0.53) Maximum thickness: 3.99	2.38 (0.90) Maximum thickness: 4.50
Shepherd et al. (37)	11 sets of cadaver joints averaging 65.1 years	Needle probe technique	Femoral condyles: 2.15 (0.39) Patellar surface: 2.23 (0.28)	Central: 2.59 (0.45) Covered by menisci: 2.01 (0.42)
F.M Hall et al. (36)	370 Adult knees averaging 34.7 years	Arthrograms using standard double-contrast techniques	Maximum thickness: Medial condyle: 4.0 (0.8) Lateral condyle: 3.7 (0.8)	/

Standard deviation (SD)
Li et al. : I = Inner, C = Central, O = Outer

2.4. Joint capsule

The joint capsule surrounding the knee joint is composed of the inner synovial membrane and the outer fibrous capsule. The synovial membrane extends to the cartilage of the knee joint and patella. The fibrous membrane is reinforced through other anatomical structures in places where strength is insufficient (figure 5) (24). Anterior reinforcement consists of the tendon of the femoral quadriceps muscle, the patella and the patellar tendon, bilateral flanked by the patellar retinaculum. The meniscopatellar and medial and lateral patellofemoral ligaments form a deep reinforcement. Anterolateral and medial muscular reinforcement is provided by the vastus muscles, the sartorius muscle, the femoral biceps muscle and the iliotibial tract. The medial collateral ligament (MCL) confers medial reinforcement. The joint capsule is posteriorly thin and reinforced by the popliteus muscle, the gastrocnemius muscle, the oblique popliteus ligament (the diagonal extension of the semimembranosus muscle from the lateral epicondyle) and the arcuate popliteal (from the femoral lateral epicondyle to the caput fibulae) (figure 9). The latter is a reinforcement by the popliteus tendon (22, 24, 45).

The synovial membrane extends upward into the suprapatellar bursa, deeply from the quadriceps muscle. Additional bursas in the knee joint include subcutaneous prepatellar bursa, subcutaneous and deep infrapatellar bursa, popliteal bursa, deep bursa of the medial head of the gastrocnemius muscle, semimembranosus bursa, bursa of the lateral collateral

ligament (LCL), pes anserine bursa, femoral biceps bursa and bursa of the iliotibial tract (figure 5) (24, 46). The infrapatellar synovial plica is located anterior to the intercondylar fossa of the knee. Anterior to the plica is the infrapatellar fat pad, dorsally from the patellar tendon (24).

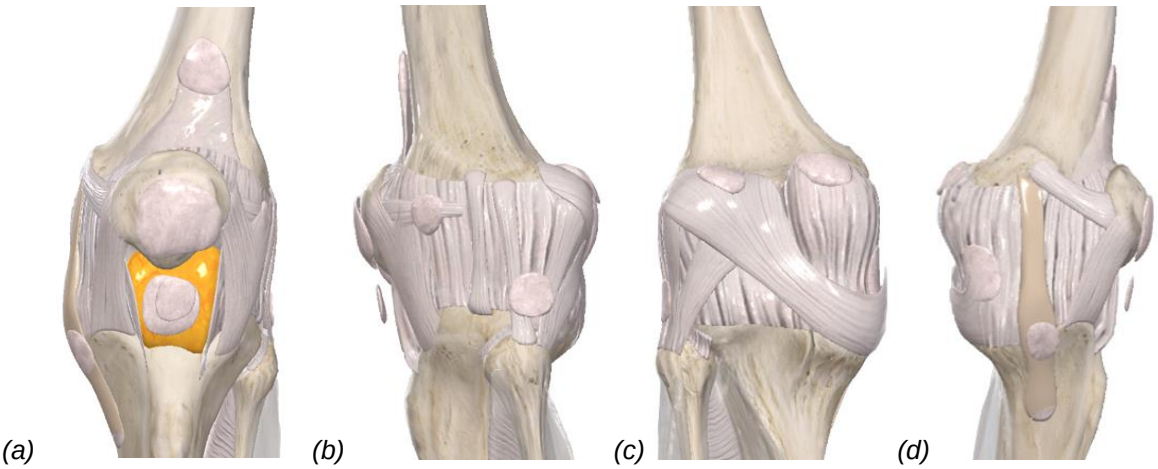

Figure 5: (a) Anterior coronary view, (b) lateral sagittal view, (c) posterior coronary view and (d) medial sagittal view of the left knee with connective tissues. The connective tissues are grey, the bursae are light grey structures on top and the infrapatellar fat pad is the orange structure visible in (a). The bursa deep of the LCL is not visible (25).

2.5. Cruciate ligaments

The anterior cruciate ligament (ACL) attaches to the anterior intercondylar area of the tibia, and the intercondylar fossa of the lateral femoral condyle. The posterior cruciate ligament (PCL) originates at the posterior intercondylar area and attaches to the lateral side of the medial femoral condyle (figure 6) (22-24, 47).

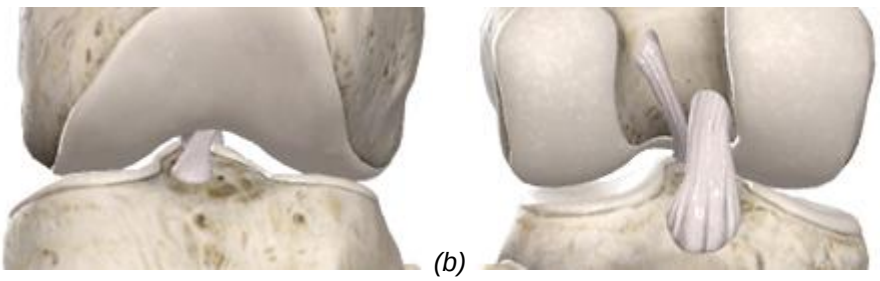

Figure 6: Anterior (a) and posterior (b) coronary view of the left knee with cruciate ligaments (25).

2.6. Meniscus

The menisci are 2 separate fibro-cartilaginous discs, dense ECM, located between the articular surfaces of the femur and tibia. Both menisci have an anterior and posterior horn and form an incomplete horizontal septum in the articular cavity. The transverse intermeniscal ligament connects the two menisci anteriorly (figure 7). The outer edge of the menisci is thick

and convex, becoming thinner and concave toward the centre. The centre of the tibial plateau remains uncovered by meniscal tissue (22-24, 48, 49).

The medial meniscus is C-shaped and occupies 51% to 74% of the medial tibial plateau (22, 48). The posterior horn is attached anteriorly to the attachment of the PCL in the posterior intercondylar fossa of the tibia. The anterior horn is usually attached to the flat part of the intercondylar region anterior to the ACL. The other sites of connection vary between the downward slope of the medial articular plateau to the intercondylar region and on the anterior slope of the tibial plateau. The peripheral edge of the medial meniscus is additionally fixed by the coronary ligament, a connection of the meniscus to the joint capsule, and the MCL (48, 49).

The lateral meniscus covers 60 - 93% of the lateral tibial plateau with its almost uniform round shape. The anterior horn is attached to the intercondylar fossa, anterior to the intercondylar eminence and posterolateral to the insertion of the ACL. The posterior horn is attached to the intercondylar eminence between the lateral tibial spine and the posterior horn of the medial meniscus (24, 48, 49). The lateral meniscus is not fixed by the collateral ligament, making it more mobile. The medial fibres of the popliteus muscle inscribe on the lateral meniscus and regulate the mobility of the meniscus relative to the femur, along with the meniscofemoral ligaments. The anterior and posterior meniscofemoral ligaments run respectively anterior and posterior to the PCL and can additionally fix the posterior horn of the lateral meniscus to the PCL and medial femoral condyle (figure 7) (23, 24, 48, 49).

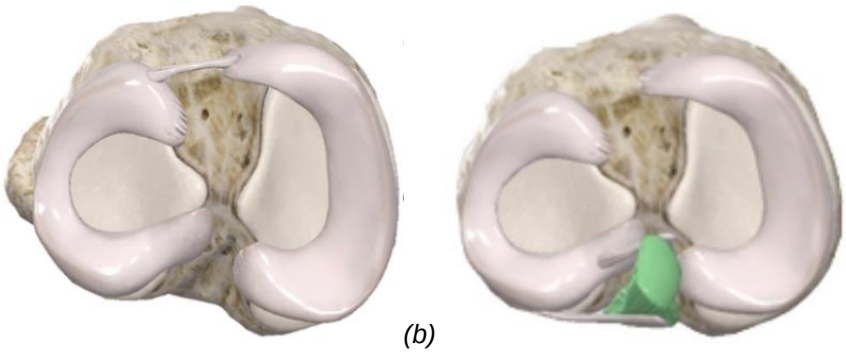

(a) *(b)*

Figure 7: Axial view on the tibia plateau of a left knee. (a) Medial and lateral meniscus and intermeniscal ligament in light pink. (b) Medial and lateral meniscus in light pink. The PCL highlighted in green for visualization of the anterior and posterior meniscofemoral ligaments, the light pink ligaments respectively anterior and posterior to the PCL (25).

2.7. The medial and lateral collateral ligament

The flat triangular MCL is attached to the medial femoral epicondyle, just below the adductor tubercle, and to the tibia. The posterior part of this MCL attaches to the shaft of the tibia whose deep fibres continue into the joint capsule and fix the medial meniscus (figure 8) (22-24).

The LCL has a cord-like shape originating on the lateral femoral condyle anterior to the gastrocnemius (figure 8). It inserts Y-shaped on the caput fibula over the insertion of the femoral biceps muscle. The interposition of the popliteus muscle between the LCL and the lateral meniscus prevents the 2 structures from connecting and makes the ligament located extra-articularly (22-24).

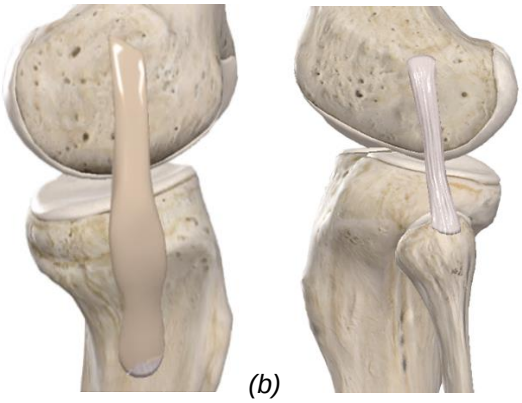

(a) *(b)*

Figure 8: Medial (a) and lateral (b) sagittal view of the left knee. (a) MCL is illustrated in brown. (b) LCL is illustrated in grey (25). The LCL is lacking the Y-shaped insertion.

2.8. The popliteus muscle

The popliteal muscle is triangular. Its origin is broad, localized proximally on the medial tibial surface. The muscle progresses superolaterally through the popliteal hiatus to intra-articular. The superficial fibres of the muscle attach to the joint capsule, the deep ones to the lateral meniscus. The popliteofibular ligament anchors the tendon with the fibular head (figure 9) (24, 50).

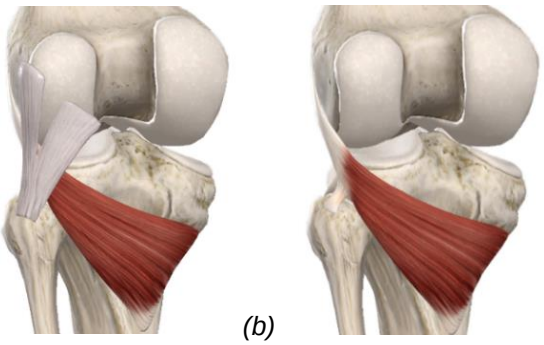

(a) *(b)*

Figure 9: Posterior coronary view on the left knee. (a) Popliteal muscle (red) with arcuate popliteal ligament (grey). (b) Popliteal muscle with popliteofibular ligament (white) (25).

2.9. Quadriceps mechanism and patellar tendon

The patellar tendon, averaging 4.6 cm in length and 8.5 mm in width, extends from the inferior pole of the patella to the tibial tuberosity, lateral ago from the long axis of the tibia (27). The quadriceps muscle consists of the intermediate, medial and lateral vastus and femoral rectus

muscles which attach proximally to the patella (figure 10). Before the insertion, the 4 muscles form tendons that may join. The intermediate vastus muscle inserts dorsally on the patella. The medial and lateral vastus muscles attach ventrally from the intermediate muscle. The most eccentric fibres of both muscles attach to the side of the patella, run along the patella directly to the patellar tendon, are part of the patellar retinaculum or cross the patella anteriorly and attach to the condyle of the tibia. The femoral rectus muscle inserts on the upper third of the anterior surface of the patella. The anterior fibres run directly across the patella to fuse with the patellar tendon (27, 45). The course of the quadriceps muscle forms a quadriceps angle (angle Q) defined as the angle between the lines connecting the middle of the patella to the anterior superior iliac spine and the tuberosity of the tibia (figure 10) (23, 24).

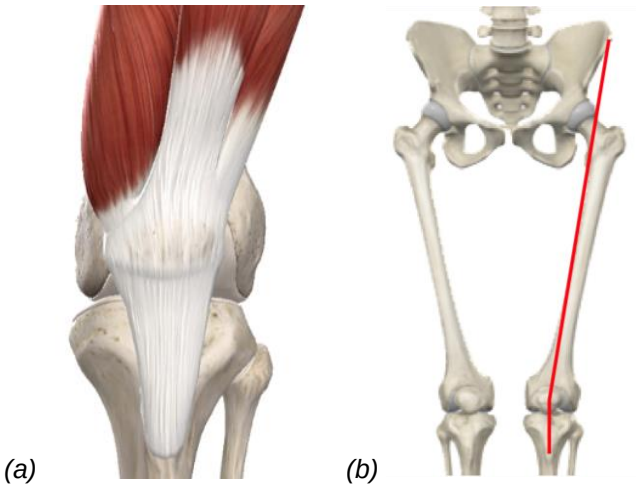

Figure 10: (a) Anterior coronary view on the left knee with quadriceps mechanism (red) and patellar tendon (white). (b) Anterior coronary view on the left angle Q. The dark red lines follow the course of the quadriceps muscle, going from the anterior superior iliac spine, through the middle of the patella, to the tuberosity of the tibia (25).

3. Biomechanics of the knee

3.1. Static information

The mechanical axis of the leg is defined as the line connecting the centre of the femoral head and the middle of the ankle. This axis normally runs centrally through the knee joint. The femoral diaphysis, the middle of the knee and the tibial shaft represent the anatomic alignment, an opened angle of 172-177° (figure 11). This anatomic axis constitutes a physiological valgus angle of the knee when the mechanical alignment is 180° (23, 24).

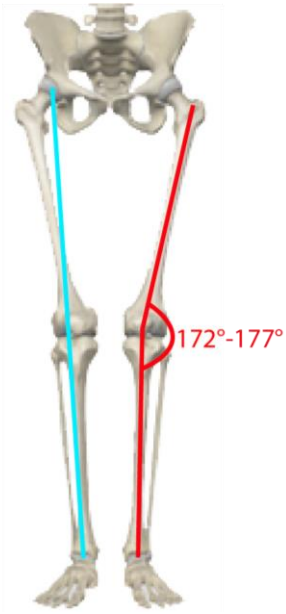

Figure 11: Anterior coronary view on the right mechanic axis and left anatomic axis. Mechanic axis: The blue line through the femoral head, the centre of the knee joint and the middle of the ankle. Anatomic axis: The red lines follow the axis of the femur and tibial shaft, going through the middle of the knee. The formed angle is indicated by an arc (25).

3.2. Stability

The geometry of the joint surfaces, ligaments, capsule, muscles, cartilage, synovial tissue, synovial fluid and other connective tissues are necessary for the mobility and stability of the knee. These structures interact with each other. The stability of the knee is optimal in extension, primarily due to the shape of the femoral condyles. The muscles around the knee are major stabilizers, mainly the medial and lateral vastus muscles. The ACL, PCL, MCL and LCL follow these muscles in importance (22-24). The primary function of the cruciate ligaments is anterior-posterior stabilization of the flexed knee. The ACL prevents posterior translation and the PCL prevents forward displacement of the femur relative to the tibial plateau (22-24, 47).

The medial and lateral retinaculum, the closely associated patellofemoral ligaments and eccentric fibres of the quadriceps muscle also add to joint stabilization (24, 45). Stabilization is also a main function of the popliteal muscle. The muscle facilitates external rotation of the femur relative to the tibia during loading. Furthermore, it prevents external movement of the meniscus during flexion of the knee (23, 50).

The quadriceps mechanism is an important dynamic stabilizer of the anterior knee joint (27). The patella creates an offset that increases the leverage of the knee extensors, providing

stability during loading and transferring force from the quadriceps to the tibia. The patella has a protective function for the knee joint during flexion (22, 23, 27).

The menisci are important for the function and maintenance of the knee joint by creating better congruency, static stabilization, friction reduction, load transfer and even pressure distribution on the articular cartilage by creating a larger bearing surface. Only when the knee is heavily loaded does the femur rest centrally directly on the tibia. The menisci provide lubrication and nourishment by spreading a layer of synovial fluid over the joint surfaces (22-24, 48, 49).

3.3. Directions of motion

The largest joint in the body, the knee, is a “modified” hinge joint. In addition to being a hinge joint, the knee is also a rolling joint due to the limited congruence of the joint surfaces (23, 24). The most extensive movement is flexion-extension. There are 4 supplementary directions of movement in the knee joint: internal-external rotation and adduction-abduction. The tibia can additionally move relative to the femur in the sagittal plane, in the coronal plane and inferior-superior. These movements are determined and limited by the conformation of the enveloping soft tissues. The main ligamentous structures here are similar to the 4 providing stability. Ligaments prevent abnormal and limit physiological movements (22-24). Friction between structures during movement of the knee is reduced by bursae using synovial fluid produced by the synovial membrane (24, 46). The infrapatellar synovial fold, a fat-filled fold, provides lubrication to the joint and prevents the capsule from folding inward (24).

Flexion movement of the knee occurs by “roll back” and sliding of the femur relative to the tibia (23). This movement is limited by the contact between the calf and femur (24). Active flexion can obtain an angle of 140°. Passively, the flexion angle can reach 160°. During flexion, angle Q increases due to internal rotation of the tibia and lateralization of the patella. Extension causes pinching of the menisci between the joint surfaces (23). The two collateral ligaments have a dorsal location of the femoral, tibial and fibular axes that causes them to relax on flexion and tighten on extension. They provide resistance at extension above 5 to 9° (24). The opposite effect is obtained by the superficial anterior fibres of the MCL (23). The extension is accompanied by external rotation of the tibia relative to the femur (23, 24). At the end of the extension, internal rotation of the tibia inevitably occurs (24). Overextension of the knee is prevented by both cruciate ligaments (23).

Rotation of the knee occurs between the tibia and the menisci. The lateral meniscus follows the rotation, the medial deforms (24). Rotation is limited by the collateral ligaments, cruciate ligaments and popliteus muscle. Internal and external rotation is only possible during flexion.

The MCL limits tibial external rotation and anterior translation. The LCL limits internal rotation. Both cruciate ligaments stretch during, and thus limit, internal rotation. The popliteal muscle limits external rotation (22-24).

Abduction and adduction are significantly limited by the collateral ligaments, ACL and popliteus muscle. The MCL prevents deviation during valgus loading of the knee, the LCL prevents varus position (22-24).

3.4. Cartilage

The cartilage in the knee joint causes minimal friction and simplifies the transfer of load to the subchondral bone. Cartilage enables joints to be loaded repeatedly (30). Proteoglycans of the cartilage, in interactions with the interstitial fluid, provides compressive resilience during static loading. The collagen network modulates mechanotransduction by tensile, push and frictional forces (30, 31). These develop a solid matrix that optimally resists tensile, compressive and shear forces during dynamic and static loading of the joint (31). The orientation in de superficial layer causes maximum stresses during compression and movement of the joint. Tensile stiffness and strength are strongly related to the orientation of the fibres relative to the applied stress (32). The middle layers play a role in shock absorption. The deepest layer is responsible for anchoring the cartilage to the bone (33). Chondrocytes are responsible for the homeostasis of cartilage (30). The homeostasis of the avascular cartilage also depends on synovial fluid and subchondral bone. The synovial fluid supplies the superficial layers with nutrients through diffusion. Deeper layers are nourished by the subchondral bone (34). The synovial fluid also has a central role in the biomechanical behaviour and lubrication of cartilage (30).

4. Osteoarthritis of the knee

4.1. Pathogenesis

OA presents a heterogeneous clinical picture of progressive mono- or polyarthritis (3). It primarily affects the hand, knee, hip and spine joints (7). An imbalance between load and load capacity disrupts the integrity of cartilage (3). Mechanical loading, biomechanical factors and genetic factors affect chondrocytes, disrupting the balance between catabolic and anabolic processes (2). The active degenerative process successively affects the cartilage and subchondral bone (6). The pathological breakdown leads to a regenerative process with sclerosis (a hypertrophic reaction) and osteophytes (bone remodelling), which maintain the catabolic processes (2). Secondary synovial inflammation develops, which can cause further tissue breakdown and pain. Eventually, the entire cartilage will break down (2, 3, 7).

Aging is the main risk factor for articular cartilage damage (3). People with mechanical joint injuries, a history of surgery on the joint, repeated overuse, joint laxity, local mechanical factors such as stance abnormalities and congenital joint defects, metabolic syndrome, a genetic predisposition or certain epigenetic factors, muscle weakness, female gender and oestrogen deficiency are more likely to develop the disabling condition. Diet and ethnicity are also thought to influence the onset of cartilage damage (2-4, 7). Biomechanical risk factors specific to OA of the knee are atrophy of the quadriceps muscle, ACL injury, meniscus injury or meniscectomy and varus or valgus position of the knees. The function of the quadriceps muscle as a pressure buffer and patella stabilizer is impaired by atrophy of the muscle. An ACL or menisci rupture possibly leads to the development of OA by initiating an acute phase response in the knee joint and altering the static and dynamic loading in the knee. The meniscus is also a shock absorber of the knee. When damaged, this protective function decreases which increases the risk of cartilage injuries. Varus and valgus positions increase the load on the medial and lateral compartments of the tibiofemoral joint, respectively, which can cause OA at these sites (51-54).

4.2. Clinic

The most characteristic symptom of OA is joint pain when loaded. This is chronic mechanical pain due to erosion of cartilage tissue causing friction between bones (2). The pathological processes lead to deformation of the joint (3). A later stage of OA leads to sagging and weakening of muscles and tendons (7, 52). The previous factors can lead to a crippling loss of function, stiffness, joint instability and activity limitations that can give rise to severe agitation and depression (2-4, 7). Radiographically, erosions at the level of articular cartilage, narrowing of the articular fissure due to cartilage loss, bone cysts, osteophytes, sclerosis, bone marrow lesions and low-grade synovitis can be identified (2, 3, 7, 55).

4.3. Imaging modalities

4.3.1. X-ray

Staging of the severity of knee OA can be based on clinical symptoms, radiological abnormalities and progression. In clinical practice, staging from radiographs is used for the primary diagnosis and progression of OA, for example the Kellgren and Lawrence classification (table 2) (52, 56, 57).

Table 2: Staging of OA of the knee after Kellgren and Lawrence (52, 56, 57).

Stage 0	Normal

Stage 1	Starting OA: incipient osteophytic lipping on eminences
Stage 2	Incipient joint space narrowing, limited subchondral sclerosis
Stage 3	Minimum halved joint space, rounded femoral condyle, extensive subchondral sclerosis, large/multiple osteophyte formations
Stage 4	Joint destruction, minimal joint space, subchondral cysts, subluxated joint

4.3.2. Magnetic resonance imaging

An MRI scan is more useful than other imaging techniques for examining soft tissue and organs (58). MRI is therefore the preferred technique for assessing cartilage (55). MRI recordings create cross-sectional images composed of voxels (59). It does not use harmful ionizing radiation for imaging, but it does use a harmless magnetic field. Another advantage is that MRI is a multiplanar imaging technique. Images can be taken in the sagittal, coronal, transverse and oblique planes. Images can be displayed in two-dimensional (2D) or 3D form (58, 60). Last but not least, depending on the settings, highly qualitative imaging is obtainable (58).

The equipment and installation for an MRI examination are expensive. Therefore, the number of examination sites is limited, resulting in a long waiting time (58). The tunnel shape, limited space and intense noise can create a claustrophobic feeling. A burning sensation at the site of a tattoo may cause additional discomfort. Moreover, it is a lengthy examination compared to other imaging techniques (58, 60). This prolonged image acquisition results in numerous images that require large storage space. The quality of the images can be disrupted by metal and motion artifacts and variations in magnetic field strength (55, 58, 60).

Metal is a barrier to MRI examinations. In the presence of movable iron- or nickel-containing objects (cerebral vascular clamp, heart valve prostheses, copper coil, metal splinter, bullet, etc.) in the body, an MRI scan is contraindicated (58, 60). Due to interference between metal and magnetic current, immobile metals (such as an artificial joint) may be a relative contraindication. All removable metals on the body should be removed (58). Similarly, implanted electrical and/or magnetic medical devices (pacemaker, defibrillator, electro stimulator, nerve stimulator, bladder stimulator, drug pumps, cochlea implants and magnetic dental implants) may be interfered with by an MRI examination. If a short shutdown of the device is possible (according to the pump's managing centre and in independent patients), the

MRI scan can still be performed if necessary. A final obstacle is a pregnancy. An MRI examination during the first pregnancy trimester is not recommended (58, 60).

4.3.3. Computed tomography arthrography

CT arthrography employs a water-soluble iodinated contrast agent which is injected intra-articularly and diffuses into the cartilage (61, 62). The integrity of the articular cartilage can be evaluated by the characteristics of contrast diffusion. CT imaging has a high sensitivity to changes in bone allowing detection of subchondral bone lesions. CT with contrast has a better resolution than MRI making subtle cartilage changes due to OA observable (62). Disadvantages of the imaging technique are the use of ionizing radiation and intra-articular contrast injection, with infection and allergy risk (61, 62).

4.4. Treatment

Interventions that cause curation or stagnation of OA are non-existent (3). The treatment goal is pain relief, improvement of quality of life and preservation of functional ability and mobility (2, 7). The severity of the debilitating joint disease determines the treatment (3). Non-pharmaceutical interventions include weight reduction, assistive devices, lifestyle modification, muscle strengthening, neuro training, exercise and aerobic training. These interventions have preventive and possibly symptom-relieving effects (2, 3, 7). Intra-articular hyaluronic acid may be considered (2). Glucosamine and chondroitin sulphate supplements are widely used notwithstanding their effectiveness is questioned (3). The pharmacologic approach to OA treats pain and joint inflammation with analgesics and corticosteroid infiltrations into the joint (2, 7).

Arthroscopic debridement of the knee can be considered in the early stages of OA. For patients with unicompartmental OA of the knee, often accompanied by a varus or valgus position, a corrective osteotomy is a possible procedure. Depending on the malalignment location and the surgical expertise, a wedge is either cut out or inserted in the proximal tibia, distal femur or in both, to neutralize the lower limb alignment. The weight-bearing part of the joint is thereby moved from the arthritic to the healthy compartment possibly resulting in pain relief, functional improvement, slowing of OA progression and postponement of joint replacement surgery (63). Arthroplasty is the final treatment (3, 63).

The hypothesis of the study

1. Long-term approaches and goals

The long-term approach of this study is to design a personalized musculoskeletal and biomechanical model of the knee based on statistical analyses of data from a gait analysis and MRI examination. This will allow the force and pressure distribution in the knee joint and soft tissue anatomy to be accurately predicted in clinical settings. This model can estimate the biomechanical risk of OA although risk factors and OA do not have a one-to-one relationship. Prevention in high-risk individuals will be able to delay or prevent the development of OA. Relying on the prediction, a more correct diagnosis could be made, and if necessary, a more optimal surgical treatment could be applied.

To achieve the biomechanical goal, a 3D model of the knee anatomy must first be created from 2D CT or MRI images. With these models and the results of gait analysis, a script will be developed to predict the force and pressure distribution in the knee joint.

2. Student's task

This experimental master's thesis focuses on the cartilaginous anatomy of the knee, specifically the right distal femur. The investigation of kinetics in the knee joint and other anatomical structures of the knee, both parts of a comprehensive study, are not discussed in this thesis. For the current study, a total of 60 healthy subjects were recruited by students and doctoral students. In the first 4 months, the students were expected to set up a Cally® where subjects could designate a day they wanted to participate, send emails with information about the study day and perform supportive work during MRI image acquisition. During the later time frame of the master's thesis, the distal parts of the femur, the proximal parts of the tibia and the cartilage of the femur were segmented in the Mimics® software. The final step was to perform a validation study of predicted cartilage geometry.

Materials and methods

1. Study population

The number of subjects was based on the study by J. Van Houcke et al. in which 57 subjects participated to predict personalized kinematics in the hip during squatting (64). This number of subjects proved sufficient to predict the kinetics of a movement that is more complex than walking, which will form the studied kinetic action in this work. With 60 subjects, the expectation was to have sufficient information to reliably predict the anatomy at the knee level and kinetics during walking. 30 subjects are sufficient for the validation study of knee cartilage mapping.

1.1. Inclusion criteria

The inclusion criteria in this study were complaint-free and mobile subjects in order not to distort the results of the gait analysis. Male and female subjects between 18 and 50 years old were included. The age limits were set because younger knees may be immature and the risk of cartilage lesions increases with age (3, 65).

1.2. Exclusion criteria

The following exclusion criteria were maintained: a history of surgery of the hip, knee or ankle, intra- and extra-articular fractures of hip, knee or ankle in the past, known cartilage damage in one of the weight-bearing joints, recurrent patellar luxation's, ankle laxity after multiple sprains, presence of contraindications for MRI (Introduction – 4.3.2), diabetic foot disease or neurological conditions that interfere with a smooth gait pattern. Individuals scoring 3 or more on the visual analogue scale for pain (VAS-p) at either the hip, knee or ankle at the time of inclusion were excluded. The VAS-p score is a linear measurement scale where individuals indicate the degree to which they experience pain (66).

1.3. Recruitment

The recruitment of subjects was done by distributing a flyer (appendix C). The inclusion and exclusion criteria were presented to potential participants to verify eligibility. The contact details and some demographic data of suitable subjects were stored after pseudonymization. The demographic data requested included age, height and weight. These last two characteristics are important for the settings of the MRI device. Contact details were given to participants where they could go with questions. Prior to the study initiation, participants received an e-mail with the exact time and location of their participation, the expected time frame and a request to bring non-reflective shorts. These shorts were necessary in order not

to interfere with the gait analysis results. All subjects signed an informed consent before gait analysis. Required documentation pre- and post-MRI scanning was filled (appendix D, E and F).

2. Data collection

During gait analysis, the gait pattern was recorded on a flat surface and an ascending and descending slope requiring reflective markers at certain anatomical points. These markers were placed on predefined anatomical landmarks marked on the body. During the MRI examination, paintballs were taped to exactly these markings. Through imaging, the true anatomical landmarks of the gait analysis were determined ensuring proper analysis of kinetics.

2.1. Kinetic reference points

Kinetic markers were used for gait analysis. There were 54 markers placed, 27 on each leg (figure 12 and table 3).

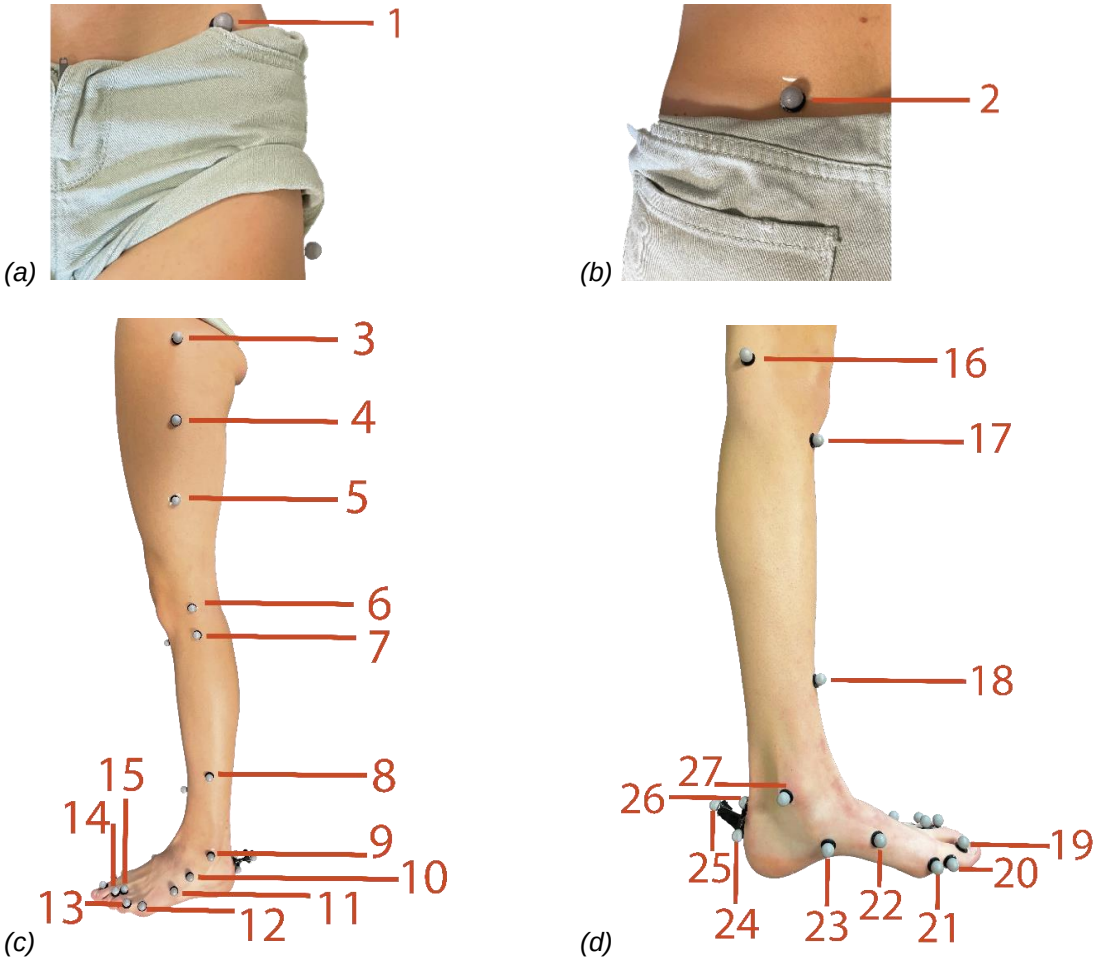

(a) *(b)* *(c)* *(d)*

Figure 12: Kinetic marker protocol visualized on the left leg of subject 30 (table 3). (a) Frontal coronary view of the left hip. (b) Posterior coronary view of the left hip. (c) Lateral sagittal view of the left leg. (d) Medial sagittal view of the left lower leg.

Table 3: Kinetic marker protocol – the legend by figure 13.

1	Left anterior superior iliac spine
2	Left posterior superior iliac spine
3	Left upper ⅓ of the thigh
4	Left thigh (middle lateral ⅓ of the thigh, just below swing of the hand)
5	Left lower ⅓ of the thigh
6	Left knee (lateral epicondyle, 1,5 cm above the joint line)
7	Left head of the fibula
8	Left lateral lower shank (⅓)
9	Left lateral malleolus
10	Left lateral calcaneum (same distance from the heel as the sustentaculum tali)
11	Left lateral border of the base of the 5th metatarsal
12	Left lateral border of the head of the 5th metatarsal
13	Left dorsal over the interphalangeal joint of the 5th digit
14	Left dorsal over the interphalangeal joint of the 3th digit
15	Left dorsal over the metatarsophalangeal joint of the 3th digit
16	Left medial femoral condyle
17	Left tuberositas tibiae
18	Left 3-4 cm above the ankle joint centre
19	Left dorsal over the hallux
20	Left medial border interphalangeal joint of the 1st digit
21	Left medial border of the head of the 1st metatarsal
22	Left medial border of the base of the 1st metatarsal
23	Left sustentaculum tali (same distance from the heel as lateral calcaneum)
24	Left inferior heel
25	Left posterior wand marker calcaneus
26	Left superior heel
27	Left medial malleolus

2.2. MRI reference points

The MRI and kinetic reference points corresponded. Additional markers were positioned at 2 transition zones of the scan blocks. The first zone was determined by measurements of 30 and 40 cm down from the highest point on the iliac crest, parallel to the leg. In this created zone of 10 cm, 9 additional paintballs were pasted: 3 laterally and 3 medially on 1 leg from anteroproximal oblique to posterodistal and 3 medially in a similar manner on the other leg. The second overlap zone was created on the lower leg by measuring 40 cm downward from the 2 boundary points of the first zone. Again, 9 MRI markers were pasted in a similar manner (figure 13).

Figure 13: Placed MRI markers visualized on the left leg of subject 30. (a) Frontal coronary view of the left hip. (b) Posterior coronary view of the left hip. (c) Lateral sagittal view of the left leg. (d) Frontal coronary view of the left leg.

2.3. Positioning

The subjects were placed in a supine position on the MRI table with the feet facing the MRI opening. A pillow was placed under the head and towels over the legs to make the approximately 45-minute scan more comfortable and prevent cold. The legs were placed on a leg rest. The feet were placed just over the edge of the leg rest. For optimal detection of the MRI signal and reduced range of motion, a body coil was placed over the abdomen and hips

and a peripheral leg coil was placed over the legs, both as close to the body as possible (58). The isocentre of the body coil had to be centrally located between the left and right hip bones. The toes were inserted through one of the lower openings of the peripheral coil so that dorsiflexion of the foot was comfortably obtained. The localization laser was placed between the feet of all subjects so that everyone was brought to the centre of the MRI tube in the same way.

2.4. Scan settings

The examination required an image from the iliac crest to the feet. Based on the applied MRI markers, 4 scan blocks were created with a sufficiently large overlapping zone allowing to complete the lower limb. In the sagittal plane, 3 scan blocks of 40 cm each were created to image the leg from the upper point of the iliac crest to the heel. The fourth scan block was taken obliquely, parallel to the axis of the foot. Flash images, some lower quality cross sections, preceded the actual scan. The aim was to check the positioning of the subjects and reset the scan blocks if necessary. Due to the positioning on the table, the MRI was set to supine - feet first.

2.5. Used sequences

The SIEMENS/Prisma_fit scanner with a 3 tesla magnetic field from UZ Ghent was used for the study. The MRI was adjusted to certain sequences needed for the study (table 4).

Table 4: Details of the MRI sequences.

Sequence	Thickness of slices (mm)	Repetition time (ms)	Echo time (ms)	Pixel (mm)
Optimisation of magnetization-prepared rapid gradient echo (MP-RAGE)	0.900	2200	2.62	0.904018

3. Data processing

3.1. Segmentation of the knee

Mimics Medical 21.0® was used for the segmentation of the knee. Classic manual staining was preferred as the segmentation method of the distal part of the femur, the proximal part of the tibia and the right femoral cartilage from the second scan block. To start the segmentation, a new mask was added whose predefined threshold was set to the maximum. This mask was used for the multiple-slice operation that was set to LiveWire and Auto-interpolate (appendix G).

3.1.1. Bones

The segmentation of the femur and tibia were marked on the contours of the cortex (figure 14 and 15). Mimics® automatically drew the line between two consecutive manually placed points. Approximately 30 and 25 points were placed per slice for the femur and tibia, respectively. If it was observed that mimics® did not follow the correct lines, the cortex was manually outlined by hovering the cursor over the edge. Of the 240 slices created, of which about 1/3 contained bone, an average of 35 were manually coloured. Intermediate slices were automatically coloured by setting auto-interpolation. Since the study focuses on the cartilage in the knee joint, extra attention was paid to correctly segment the epiphyses.

(a) 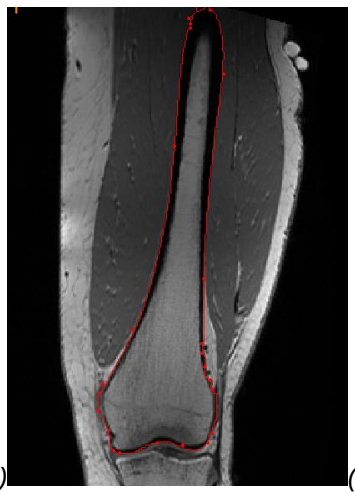 *(b)* 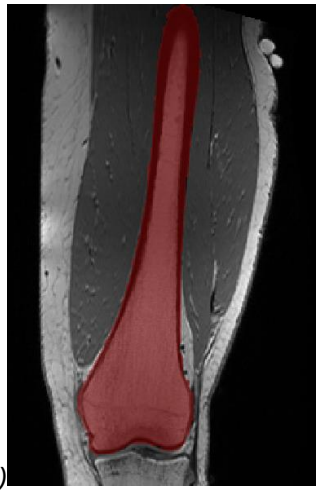

Figure 14: Segmentation of the left femur of subject 18. (a) Outlining the femoral cortex. (b) Completely segmented slice.

(a) 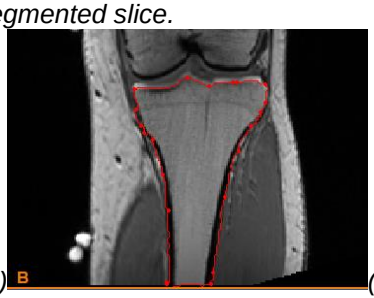 *(b)* 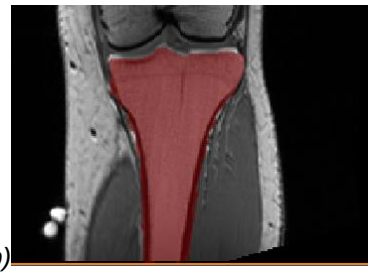

Figure 15: Segmentation of the left tibia of subject 18. (a) Outlining the tibial cortex. (b) Completely segmented slice.

To obtain the desired 3D model, the part was calculated with optimal quality. To obtain a realistic bone, the angular calculated 3D bone was smoothed (figure 16).

Figure 16: The frontal coronary view of the left femur (yellow) and tibia (blue) of the smoothed calculated parts of subject 18.

3.1.2. Femoral cartilage

The segmentation of the right femoral cartilage was obtained similarly to the segmentation of bones (figure 17). This involved following the contour of the cartilage. The segmented cartilage was viewed sagittally, coronally and axially and optimised if necessary. Approximately, each slice was segmented individually. The same additional steps were followed as for bone to obtain a 3D model (figure 18).

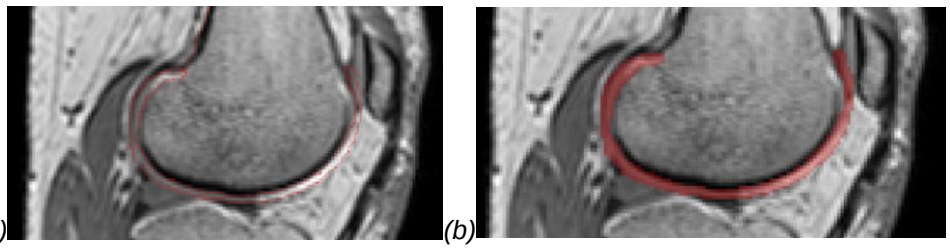

Figure 17: Segmentation of the right female cartilage of subject 5. (a) Outlining the cartilage edge. (b) Completely segmented slice.

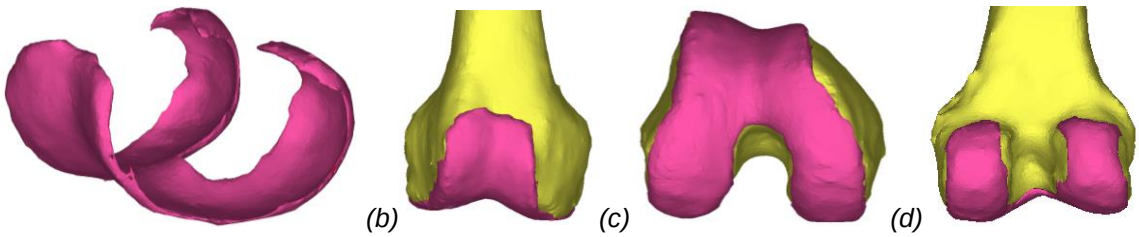

Figure 18: Smoothed right 3D cartilage model of subject 5. (a) The left front oblique view of the femoral cartilage (pink). (b) The anterior coronary view, (c) inferior axial view and (d) posterior coronary view of the distal femur (yellow) and cartilage.

4. Creating full legs

The available SSM of the complete lower limb, as developed by Audenaert and colleagues (67), was fitted on the 3D subject-specific osseous structures in the development of a subject-specific, osseous full lower limb model.

5. Automatic femoral cartilage prediction

The cartilage mapping was based on average cartilage thickness measurements. By way of manual segmentation and following averaging, an average node-specific thickness map was developed. For subject-specific cartilage prediction, this average cartilage thickness map was scaled by femoral length. For every node, the cartilage is modelled by moving the specific node over a scaled, node-specific distance along the node-specific normal (figure 19) (13). Opposing a 0 mm thickness on the nodes located at the edges, the cartilage blended smoothly into the bone. The mean femoral cartilage thickness of the prediction model was 1.41 mm with a range of 0.37 to 3.08 mm. Maximum local cartilage thicknesses were located at the patellofemoral joint surface and the posterior condyles.

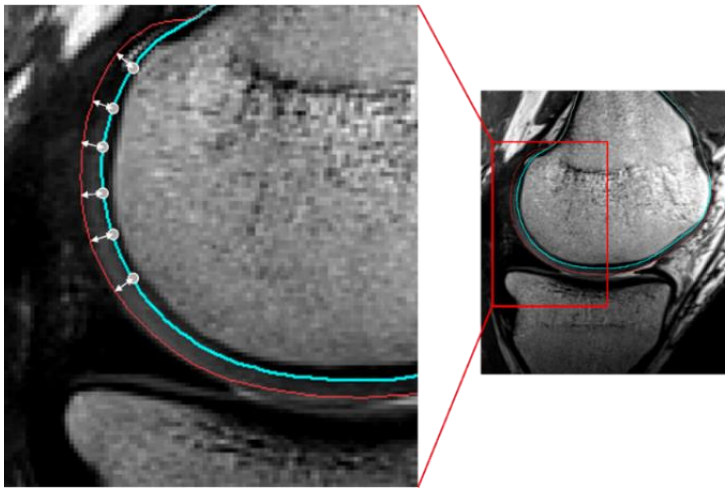

Figure 19: Detail image on MRI of the sagittal view of the femoral condyle. The vertex (blue line) and cartilage surface (red line) from the node-specific cartilage thickness along the normal of the vertex.

6. Validation automatic prediction vs. manual segmentation

To validate the above-described method for cartilage prediction, Mimics®, MeshLab® and MatLab® were used. The distal femur and distal femoral cartilage were considered as 1 entity for which the segmented piece of the femur with the cartilage in Mimics® must be merged. This was done by selecting the 2 necessary masks and performing a boolean unite operation. The obtained 3D structure is opened in MeshLab® where duplicate faces and vertices were removed.

For the 30 included subjects, the RMSE (square root of the average of all absolute squared distances, the deviation size/ accuracy), the ASD (the average of all surface distances) and the HD (the maximum absolute distance) were calculated between the cartilaginous coordinates obtained from manual segmentation and the predicted coordinates of the cartilage layer, using a MatLab® script.

7. Statistical analysis

The normality of the 30 case-specific values was verified. The RMSE, ASD and HD values were imported into SPSS® and the Shapiro-Wilk test was performed.

Results

1. Study population

Recruitment of subjects yielded 81 persons. Of these, 38 subjects were scheduled for the 8 study days that were conducted. During the course of the study, 4 subjects dropped out due to difficulties in the gait analysis, a possible pregnancy and 2 did not show up at the appointment. This validation study was eventually administered to 30 randomly selected healthy adults. Only 1/5 of the subjects were women. The mean demographics of the study population were 23.5 years in age, 179.22 cm in height and 69.73 kg in weight. The department of orthopaedics at UZ Ghent used a dataset of 53 Caucasian males between 17 and 25 years of age without obesity, a mean body mass index of 21.70 kg/m^2 and a mean height of 181.79 cm to develop the SSM.

2. Statistical analysis

The 30 case-specific RMSE, ASD and HD values had a significance of respectively 0.005, 0.002 and 0.324 following a Shapiro-Wilk test.

3. Validation of cartilage thickness prediction

For validation of the right distal femoral cartilage prediction, the median and ranges of the RMSE, ASD and HD were calculated and interpreted (table 5). Point-dependent deviations were assessed (figure 20).

Table 5: RMSE, ASD and HD of right femoral cartilage prediction: median and range (mm).

	Femoral cartilage
RMSE (range)	0.6723 (0.4947 – 1.2132)
ASD (range)	0.5580 (0.4303 – 1.0251)
HD (range)	2.4165 (1.3110 – 4.4678)

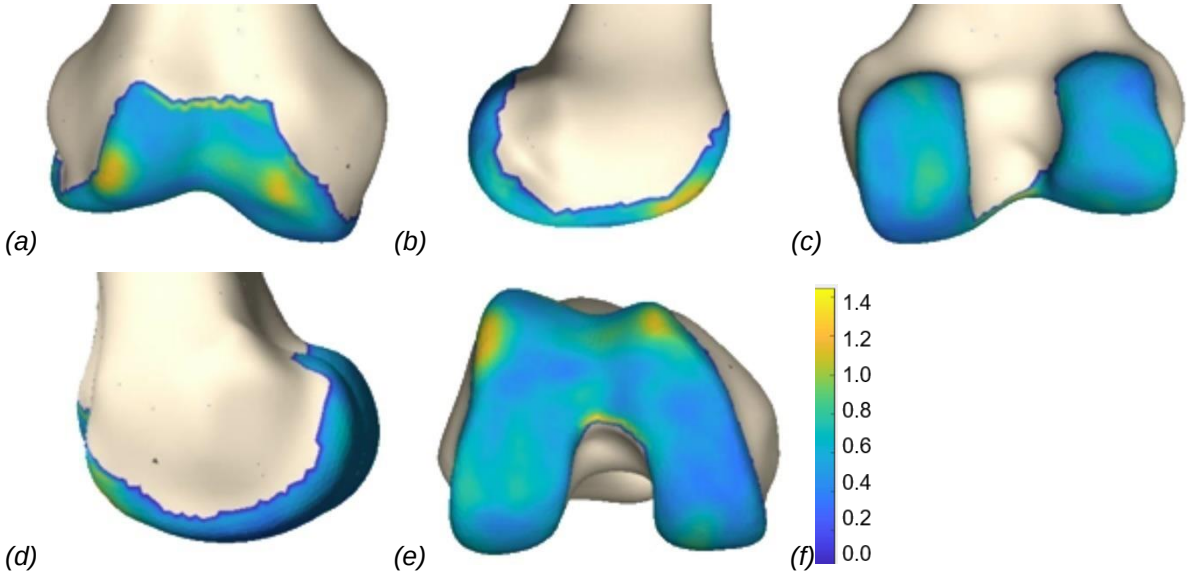

Figure 20: Visual representation of the mean point-dependent error for right femoral cartilage. A right distal femoral epiphysis in (a) frontal coronary view, (b) lateral sagittal view, (c) posterior coronary view, (d) medial sagittal view and (e) distal axial view. (f) The colour code represents the mean error with blue representing an error of 0 mm and yellow representing an error of 1.4 mm.

Discussion

OA is the most common chronic joint disease and its prevalence is increasing (2, 4). Knee OA constitutes 83% of the global disease burden for OA (5). Mechanical stress on the knee is an important risk factor (3). Computational musculoskeletal modelling becomes more popular for the non-invasive estimation of joint loading distribution (9, 10). Typically these methods depend on cumbersome and time-consuming manual segmentation of joint geometry (11, 12). An SSM that predicts anatomical architecture based on imaging can overcome this impediment. The current study validated an automated method for personalized distal femoral cartilage mapping developed within the department of orthopaedics at UZ Ghent. The methodology and results were presented in this study.

The choice was made to represent the median instead of the mean based on the non-normally distributed RMSE and ASD. Additionally, the range is displayed which presents extreme values. The median of all subject-specific ASDs is 0.5580 mm. This is the error relative to the local cartilage thickness. The median RMSE is 0.6723 mm. This value is a sensitive measure of large errors and outliers because of its quadrature. These deviations are tolerable. Nonetheless, the median HD of 2.4165 mm indicates that optimisation of the cartilage mapping is further required. Despite the high HD values, the average error is relatively low. Thus, there is a large distribution in the accuracy of node-specific prediction in a subject. The range of the RMSE (0.4947 - 1.2132 mm), ASD (0.4303 - 1.0251 mm) and HD (1.3110 - 4.4678 mm) indicate a large interpersonal variation. The cartilage anatomy could be more difficult to predict in certain anatomical variants. The main prediction error is located frontally, proximally and bilaterally on the femoral trochlea and distally at the location where the medial and lateral condylar cartilage meet (figure 20). The reason could be that these specific boundary thicknesses are more difficult to predict as well as the cartilage thickness on top of eminences. Based on these location-specific deviations, the automatic prediction method can be optimised. This would improve all calculated values in the validation study.

Van Dijck and colleagues (18) also used a point distribution model to create an SSM of the tibiofemoral joint. Their study group consisted of 524 patients with a median age of 66 years. This population already has an increased risk of cartilage damage making the used age range of the validated model between 17 and 25 years more appropriate (3). The larger study population is superior to the 53 cases used in the developing model.

The actual mean cartilage thickness in the distal femur is unclear. The mean from the cartilage map used for the automatic prediction is 1.41 mm, not consistent with the values found in the literature (table 1). Including the 0 values of the transition zone from cartilage to bone in the

mean cartilage thickness may explain the lower value. None of the authors listed in table 1 measured cartilage thickness at the same locations, so comparing the values is less instructive. The values of Shepherd et al. were discussed case-specifically in the article but the mean was not shown (37). The mean shown in table 1 was calculated while reviewing the values from the article. Nevertheless, differences in cartilage thickness may find their cause in the used method. Despite Cohen et al. (41) and Li et al. (39) calculated the mean cartilage thickness using the MRI technique, which was also used for the mean value of the prediction model, the obtained results are divergent. The arthrogramming technique, possibly using MRI images, used by F.M Hall et al. (36) also shows substantial differences. Cohen et al. (41) and Shepherd et al. (37) conducted a cadaver study. Cartilage is significantly composed of water making its composition potentially altered post-mortem compared to healthy volunteers (34). The study by Shepherd and colleagues showed a wide variation in results because cadaveric specimens with already severe cartilage damage were also examined (37, 41). A large mean age difference was observed between the studies, which may affect cartilage thickness (3).

The ultimate goal of the broader study is to develop a statistical model for predicting both musculoskeletal anatomy and biomechanical factors of the knee joint. The desired study population is 60 healthy subjects, with the inclusion and exclusion criteria specified in the materials and methods section. Additional study days are desirable to achieve this goal. Studies to develop a statistical model for force and pressure in the knee joint are ongoing, which is based on an anatomical model (9, 10). The anatomical model is also being studied. A nuance of the anatomic model can be obtained by taking additional imaging with knees flexed because soft tissue morphometry can be affected by knee position.

1. Limitations

The errors in the validation study should not be immediately attributed to the automatic prediction. This prediction is based on the distal femoral morphometry and whole femur length. The proximal part of the femur, required for the automatic prediction, was completed by an SSM (67). This works accurately but minimal variations may occur that were not taken into account in the validating population. A validation study using a fully manually segmented leg could overcome this potential interfering factor but would become more time-consuming. The scan blocks created in this study must be merged to obtain a full leg. A more likely explanation for the errors is the manual segmentation of both bone and cartilage in the prediction model and validation study that may be inaccurate (11, 12). Gougoutas et al. reported a coefficient of variation for manual segmentation of cartilage of 3.0% and 8.8% for intra-operator and inter-operator abnormalities respectively (68). Preventing operator-dependent errors could help optimise cartilage prediction. A time-consuming solution could be that 2 separate operators

segment the same cases of which the average is used for the study. Since the prediction model represents an average cartilage architecture and extreme deviations in healthy subjects are unlikely, the prediction model could validate the quality of manual segmentation.

An invasive or radiation-rich imaging technique cannot be used responsibly in healthy subjects, so MRI was preferred. Additionally, MRI appears to be the key imaging tool for OA (55). Nevertheless, the spatial resolution in the study was insufficient to accurately distinguish cartilage from bone or cartilage from each other. Parts of cartilage were segmented as bone and *vice versa,* certain voxels were incorrectly not counted as bone or cartilage and voxels outside anatomical structures were counted as bone or cartilage because of the large voxel size. The sides of the voxels of the images used for the validation study are 0.904018 mm (table 4). This makes an error of about 1 mm likely when a voxel extra or less is added to the anatomical structure. This inaccuracy was facilitated by counting the entire voxel to bone or cartilage when only a part of it was segmented. By following the outline of cubes to capture the contours of anatomical structures, the result of manual segmentation was angular. A small error remained after smoothing. A validation study on higher-quality images seems to be required.

The prediction model is based on 53 Caucasian males between 17 and 25 years of age without obesity and with an average height of 181.79 cm. These may not be representative of the entire population. Global generalization of the prediction model is debatable given genetic, cultural and environmental differences. Gender extrapolation is also arguable given the higher risk of OA in women (2). Cartilage thickness decreases with age making this factor to be incorporated when applied in clinical practice (4). Weight also affects cartilage thickness (3). The study population of the validation study consisted of Belgians, mainly men, with a mean age of 23.5 years, 179.22 cm and 69.73 kg. No subjects with a high BMI participated. Of the 30 subjects, only the right distal femoral cartilage was validated. A next validation study should include a cross-cultural study population with more women and greater weight discrepancies examining the left distal femoral cartilage as well.

2. Strengths

By fully manually segmenting the distal femoral cartilage and the distal part of the femur, small anatomical deviations from the standard shape are detected and included in the validation study of the prediction model. These may be missed when using a SSM.

The anatomical prediction model will potentially be applied in the clinic and replace time-consuming, operator-dependent manual segmentation. Patient-specific analyses of intra-articular joint stress, forces and pressures in a biomechanical model will be more accessible

to perform. Personalized interventions will be easier to implement based on a prediction model. The individualised approach in surgery has already been proven beneficial (20, 21). MRI images, which are difficult and expensive to acquire, are not necessary for the prediction model given that CT images can be used (58).

Conclusion

OA of the knee is prevalent and expected to increase with the aging of the population and an increase in obesity. Particular anatomic and biomechanical factors confer increased risk. SSM can detect these factors more efficiently by replacing cumbersome and operator-dependent manual segmentation. Estimating joint forces on the knee and soft tissue function in the knee and predicting secondary kinematics of the knee will be possible and patient-specific joint preservation or replacement surgery of the knee will be applicable using a prediction model. These purposes require additional research. In this study, cartilage mapping of the distal femur was validated. Despite optimisation being further warranted, the validation study yielded hopeful results.

References

1. Hunter DJ, March L, Chew M. Osteoarthritis in 2020 and beyond: a Lancet Commission. Lancet. 2020;396(10264):1711-2.
2. Wittoek R.: powerpoint REUMATOLOGIE: PATHOGENESIS, EPIDEMIOLOGIE, KLINIEK EN BEHANDELING VAN OSTEOARTRITIS 2022. University of Ghent, 2022; 1-31, 63-67.
3. Sacitharan PK. Ageing and Osteoarthritis. Subcell Biochem. 2019;91:123-59.
4. Mandl LA. Osteoarthritis year in review 2018: clinical. Osteoarthritis Cartilage. 2019;27(3):359-64.
5. Vos T, Flaxman AD, Naghavi M, Lozano R, Michaud C, Ezzati M, et al. Years lived with disability (YLDs) for 1160 sequelae of 289 diseases and injuries 1990-2010: a systematic analysis for the Global Burden of Disease Study 2010. Lancet. 2012;380(9859):2163-96.
6. Boer CG, Hatzikotoulas K, Southam L, Stefánsdóttir L, Zhang Y, Coutinho de Almeida R, et al. Deciphering osteoarthritis genetics across 826,690 individuals from 9 populations. Cell. 2021;184(18):4784-818.e17.
7. Xia B, Di C, Zhang J, Hu S, Jin H, Tong P. Osteoarthritis pathogenesis: a review of molecular mechanisms. Calcif Tissue Int. 2014;95(6):495-505.
8. Sharma L, Song J, Dunlop D, Felson D, Lewis CE, Segal N, et al. Varus and valgus alignment and incident and progressive knee osteoarthritis. Ann Rheum Dis. 2010;69(11):1940-5.
9. Marra MA, Vanheule V, Fluit R, Koopman BH, Rasmussen J, Verdonschot N, et al. A subject-specific musculoskeletal modeling framework to predict in vivo mechanics of total knee arthroplasty. J Biomech Eng. 2015;137(2):020904.
10. Kang KT, Kim SH, Son J, Lee YH, Koh YG. Validation of a computational knee joint model using an alignment method for the knee laxity test and computed tomography. Biomed Mater Eng. 2017;28(4):417-29.
11. Cerveri P, Manzotti A, Marchente M, Confalonieri N, Baroni G. Mean-shifted surface curvature algorithm for automatic bone shape segmentation in orthopedic surgery planning: a sensitivity analysis. Comput Aided Surg. 2012;17(3):128-41.
12. Bae KT, Shim H, Tao C, Chang S, Wang JH, Boudreau R, et al. Intra- and inter-observer reproducibility of volume measurement of knee cartilage segmented from the OAI MR image set using a novel semi-automated segmentation method. Osteoarthritis Cartilage. 2009;17(12):1589-97.
13. Van Houcke J, Audenaert EA, Atkins PR, Anderson AE. A Combined Geometric Morphometric and Discrete Element Modeling Approach for Hip Cartilage Contact Mechanics. Front Bioeng Biotechnol. 2020;8:318.
14. Audenaert EA, Van Houcke J, Almeida DF, Paelinck L, Peiffer M, Steenackers G, et al. Cascaded statistical shape model based segmentation of the full lower limb in CT. Comput Methods Biomech Biomed Engin. 2019;22(6):644-57.
15. Audenaert A, Audenaert E. Global optimization method for combined spherical-cylindrical wrapping in musculoskeletal upper limb modelling. Computer methods and programs in biomedicine. 2008;92(1):8-19.
16. Audenaert EA, Khanduja V, Bauwens C, Van Hoof T, Pattyn C, Steenackers G. A discrete element model to predict anatomy of the psoas muscle and path of the tendon: Design implications for total hip arthroplasty. Clin Biomech (Bristol, Avon). 2019;70:186-91.
17. Peiffer M, Burssens A, Duquesne K, Last M, De Mits S, Victor J, et al. Personalised statistical modelling of soft tissue structures in the ankle. Computer methods and programs in biomedicine. 2022;218:106701.
18. Van Dijck C, Wirix-Speetjens R, Jonkers I, Vander Sloten J. Statistical shape model-based prediction of tibiofemoral cartilage. Comput Methods Biomech Biomed Engin. 2018;21(9):568-78.

19. Nauwelaers N, Matthews H, Fan Y, Croquet B, Hoskens H, Mahdi S, et al. Exploring palatal and dental shape variation with 3D shape analysis and geometric deep learning. Orthod Craniofac Res. 2021;24 Suppl 2(Suppl 2):134-43.
20. Watters TS, Mather RC, 3rd, Browne JA, Berend KR, Lombardi AV, Jr., Bolognesi MP. Analysis of procedure-related costs and proposed benefits of using patient-specific approach in total knee arthroplasty. J Surg Orthop Adv. 2011;20(2):112-6.
21. Reimann P, Brucker M, Arbab D, Lüring C. Patient satisfaction - A comparison between patient-specific implants and conventional total knee arthroplasty. J Orthop. 2019;16(3):273-7.
22. Gupton M, Imonugo O, Terreberry RR. Anatomy, Bony Pelvis and Lower Limb, Knee. StatPearls. Treasure Island (FL): StatPearls Publishing
Copyright © 2022, StatPearls Publishing LLC.; 2022.
23. Vaienti E, Scita G, Ceccarelli F, Pogliacomi F. Understanding the human knee and its relationship to total knee replacement. Acta Biomed. 2017;88(2s):6-16.
24. Audenaert E. Cursus: Anatomie van het locomotorisch systeem Partim hoofd, hals, romp en ledematen. University of Ghent - Acco, 2019; 181-192
25. Elsevier. Complete anatomy.
26. Siebold R, Axe J, Irrgang JJ, Li K, Tashman S, Fu FH. A computerized analysis of femoral condyle radii in ACL intact and contralateral ACL reconstructed knees using 3D CT. Knee Surg Sports Traumatol Arthrosc. 2010;18(1):26-31.
27. Sherman SL, Plackis AC, Nuelle CW. Patellofemoral anatomy and biomechanics. Clin Sports Med. 2014;33(3):389-401.
28. Tecklenburg K, Dejour D, Hoser C, Fink C. Bony and cartilaginous anatomy of the patellofemoral joint. Knee Surg Sports Traumatol Arthrosc. 2006;14(3):235-40.
29. Rudran B, Little C, Wiik A, Logishetty K. Tibial Plateau Fracture: Anatomy, Diagnosis and Management. Br J Hosp Med (Lond). 2020;81(10):1-9.
30. Carballo CB, Nakagawa Y, Sekiya I, Rodeo SA. Basic Science of Articular Cartilage. Clin Sports Med. 2017;36(3):413-25.
31. Halonen KS, Mononen ME, Jurvelin JS, Töyräs J, Korhonen RK. Importance of depth-wise distribution of collagen and proteoglycans in articular cartilage-A 3D finite element study of stresses and strains in human knee joint. Journal of Biomechanics. 2013;46(6):1184-92.
32. Below S, Arnoczky SP, Dodds J, Kooima C, Walter N. The split-line pattern of the distal femur: A consideration in the orientation of autologous cartilage grafts. Arthroscopy. 2002;18(6):613-7.
33. Thienkarochanakul K, Javadi AA, Akrami M, Charnley JR, Benattayallah A. Stress Distribution of the Tibiofemoral Joint in a Healthy Versus Osteoarthritis Knee Model Using Image-Based Three-Dimensional Finite Element Analysis. Journal of Medical and Biological Engineering. 2020;40(3):409-18.
34. Cheng KY, Lombardi AF, Chang EY, Chung CB. Knee Cartilage Imaging. Clin Sports Med. 2021;40(4):677-92.
35. Lewis R, Feetham CH, Barrett-Jolley R. Cell volume regulation in chondrocytes. Cell Physiol Biochem. 2011;28(6):1111-22.
36. Hall FM, Wyshak G. Thickness of articular cartilage in the normal knee. J Bone Joint Surg Am. 1980;62(3):408-13.
37. Shepherd DE, Seedhom BB. Thickness of human articular cartilage in joints of the lower limb. Ann Rheum Dis. 1999;58(1):27-34.
38. Otterness IG, Eckstein F. Women have thinner cartilage and smaller joint surfaces than men after adjustment for body height and weight. Osteoarthritis Cartilage. 2007;15(6):666-72.
39. Li G, Park SE, DeFrate LE, Schutzer ME, Ji L, Gill TJ, et al. The cartilage thickness distribution in the tibiofemoral joint and its correlation with cartilage-to-cartilage contact. Clin Biomech (Bristol, Avon). 2005;20(7):736-44.
40. Schmitz RJ, Harrison D, Wang HM, Shultz SJ. Sagittal-Plane Knee Moment During Gait and Knee Cartilage Thickness. J Athl Train. 2017;52(6):560-6.

41. Cohen ZA, McCarthy DM, Kwak SD, Legrand P, Fogarasi F, Ciaccio EJ, et al. Knee cartilage topography, thickness, and contact areas from MRI: in-vitro calibration and in-vivo measurements. Osteoarthritis Cartilage. 1999;7(1):95-109.
42. Paunipagar BK, Rasalkar D. Imaging of articular cartilage. Indian J Radiol Imaging. 2014;24(3):237-48.
43. Yao JQ, Seedhom BB. Ultrasonic measurement of the thickness of human articular cartilage in situ. Rheumatology (Oxford). 1999;38(12):1269-71.
44. Jurvelin JS, Räsänen T, Kolmonen P, Lyyra T. Comparison of optical, needle probe and ultrasonic techniques for the measurement of articular cartilage thickness. J Biomech. 1995;28(2):231-5.
45. Waligora AC, Johanson NA, Hirsch BE. Clinical anatomy of the quadriceps femoris and extensor apparatus of the knee. Clin Orthop Relat Res. 2009;467(12):3297-306.
46. Steinbach LS, Stevens KJ. Imaging of Cysts and Bursae About the Knee. Radiologic Clinics of North America. 2013;51(3):433-+.
47. Chahla J, Williams BT, LaPrade RF. Posterior Cruciate Ligament. Arthroscopy. 2020;36(2):333-5.
48. Markes AR, Hodax JD, Ma CB. Meniscus Form and Function. Clin Sports Med. 2020;39(1):1-12.
49. Fox AJ, Wanivenhaus F, Burge AJ, Warren RF, Rodeo SA. The human meniscus: a review of anatomy, function, injury, and advances in treatment. Clin Anat. 2015;28(2):269-87.
50. Jadhav SP, More SR, Riascos RF, Lemos DF, Swischuk LE. Comprehensive review of the anatomy, function, and imaging of the popliteus and associated pathologic conditions. Radiographics. 2014;34(2):496-513.
51. Georgiev T, Angelov AK. Modifiable risk factors in knee osteoarthritis: treatment implications. Rheumatol Int. 2019;39(7):1145-57.
52. Lespasio MJ, Piuzzi NS, Husni ME, Muschler GF, Guarino A, Mont MA. Knee Osteoarthritis: A Primer. Perm J. 2017;21:16-183.
53. Madry H, Kon E, Condello V, Peretti GM, Steinwachs M, Seil R, et al. Early osteoarthritis of the knee. Knee Surg Sports Traumatol Arthrosc. 2016;24(6):1753-62.
54. Lohmander LS, Englund PM, Dahl LL, Roos EM. The long-term consequence of anterior cruciate ligament and meniscus injuries: osteoarthritis. Am J Sports Med. 2007;35(10):1756-69.
55. Hayashi D, Roemer FW, Guermazi A. Imaging for osteoarthritis. Ann Phys Rehabil Med. 2016;59(3):161-9.
56. Kellgren JH, Lawrence JS. Radiological assessment of osteo-arthrosis. Ann Rheum Dis. 1957;16(4):494-502.
57. Michael JW, Schlüter-Brust KU, Eysel P. The epidemiology, etiology, diagnosis, and treatment of osteoarthritis of the knee. Dtsch Arztebl Int. 2010;107(9):152-62.
58. What is an MRI scan and what can it do? Drug Ther Bull. 2011;49(12):141-4.
59. Acquaviva R, Mangione S, Garbo G. Image-based MRI gradient estimation. Magn Reson Imaging. 2018;49:138-44.
60. Verstraete K. powerpoint editor Diagnostische en therapeutische methodieken - 3BaGenBMW_MR_2014_finaal_1_dia_per_blad. University of Ghent, 2014; 83-84,89
61. Verstraete K. powerpoint 2MaGenRadiologieMSK_Inleiding_2013_Finaal 1 PER BLAD. University of Ghent, 2013; 74-76
62. Myller KA, Honkanen JT, Jurvelin JS, Saarakkala S, Töyräs J, Väänänen SP. Method for segmentation of knee articular cartilages based on contrast-enhanced CT images. Annals of biomedical engineering. 2018;46(11):1756-67.
63. Brouwer RW, Huizinga MR, Duivenvoorden T, van Raaij TM, Verhagen AP, Bierma-Zeinstra SMA, et al. Osteotomy for treating knee osteoarthritis. Cochrane Database of Systematic Reviews. 2014(12).
64. Van Houcke J, Galibarov PE, Van Acker G, Fauconnier S, Allaert E, Van Hoof T, et al. Personalized hip joint kinetics during deep squatting in young, athletic adults. Comput Methods Biomech Biomed Engin. 2020;23(1):23-32.

65. Saggese G, Baroncelli GI, Bertelloni S. Puberty and bone development. Best Practice & Research Clinical Endocrinology & Metabolism. 2002;16(1):53-64.
66. Yan J, Zhang XM. A randomized controlled trial of ultrasound-guided pulsed radiofrequency for patients with frozen shoulder. Medicine (Baltimore). 2019;98(1):e13917.
67. Audenaert EA, Pattyn C, Steenackers G, De Roeck J, Vandermeulen D, Claes P. Statistical Shape Modeling of Skeletal Anatomy for Sex Discrimination: Their Training Size, Sexual Dimorphism, and Asymmetry. Front Bioeng Biotechnol. 2019;7:302.
68. Gougoutas AJ, Wheaton AJ, Borthakur A, Shapiro EM, Kneeland JB, Udupa JK, et al. Cartilage volume quantification via Live Wire segmentation1. Academic Radiology. 2004;11(12):1389-95.

Appendix

Appendix A: Ethics committee

Afz.: Commissie voor Medische Ethiek

Prof. dr. Emmanuel Audenaert
Orthopedie en Traumatologie
ALHIER

contact	telefoon	e-mail	
Commissie voor medische Ethiek	+32 (0)9 332 41 81	Ethisch.comite@uzgent.be	
Ons kenmerk	**Uw kenmerk**	**datum**	**pagina**
BC-10519 E08	NVT	18/11/2021	1/3

Betreft : Advies voor monocentrische studie met als titel:

Titel hoofdstudie: "Op weg naar gepersonaliseerde kraakbeenpredictie van het onderste lidmaat: Validatie van reactiekrachten en weke delen anatomie ter hoogte van de knie en enkel."

Titel thesis: Op weg naar gepersonaliseerde kraakbeenpredictie van het onderste lidmaat: Validatie van weke delen anatomie ter hoogte van de knie. Scriptie Dhooge Femke

B.U.N.: B6702021000913

Adviesaanvraagformulier Document E dd 2021-4-23 (Dhooge Femke)
Alle goedgekeurde documenten van studie met als referentie BC-10519

Advies werd gevraagd door: Prof. dr. Emmanuel Audenaert

BOVENVERMELDE DOCUMENTEN WERDEN DOOR HET ETHISCH COMITÉ BEOORDEELD. ER WERD EEN POSITIEF ADVIES GEGEVEN OVER DIT PROTOCOL OP 17/11/2021 . INDIEN DE STUDIE NIET WORDT OPGESTART VOOR 17/11/2022, VERVALT HET ADVIES EN MOET HET PROJECT TERUG INGEDIEND WORDEN.

Vooraleer het onderzoek te starten dient contact te worden genomen met HIRUZ CTU (09/332 05 00).

THE ABOVE MENTIONED DOCUMENTS HAVE BEEN REVIEWED BY THE ETHICS COMMITTEE.A POSITIVE ADVICE WAS GIVEN FOR THIS PROTOCOL ON 17/11/2021 . IN CASE THIS STUDY IS NOT STARTED BY 17/11/2022, THIS ADVICE WILL BE NO LONGER VALID AND THE PROJECT MUST BE RESUBMITTED.

Before initiating the study, please contact HIRUZ CTU (09/332 05 00).

° *Het Ethisch Comité werkt volgens 'ICH Good Clinical Practice' - regels*
° *Het Ethisch Comité beklemtoont dat een gunstig advies niet betekent dat het Comité de verantwoordelijkheid voor het onderzoek op zich neemt. Bovendien dient U er over te waken dat Uw mening als betrokken onderzoeker wordt weergegeven in publicaties, rapporten voor de overheid enz., die het resultaat zijn van dit onderzoek.*
° *In het kader van 'Good Clinical Practice' moet de mogelijkheid bestaan dat het farmaceutisch bedrijf en de autoriteiten inzage krijgen van de originele data. In dit verband dienen de onderzoekers erover te waken dat dit gebeurt zonder schending van de privacy van de proefpersonen.*
° *Het Ethisch Comité benadrukt dat het de promotor is die garant dient te staan voor de conformiteit van de anderstalige informatie- en toestemmingsformulieren met de nederlandstalige documenten.*
° *Geen enkele onderzoeker betrokken bij deze studie is lid van het Ethisch Comité.*
° *Alle effectieve leden van het Ethisch Comité, of hun plaatsvervangers,hebben dit project beoordeeld. (De ledenlijst is bijgevoegd)*
° *The Ethics Committee is organized and operates according to the 'ICH Good Clinical Practice' rules.*
° *The Ethics Committee stresses that approval of a study does not mean that the Committee accepts responsibility for it. Moreover, please keep in mind that your opinion as investigator is presented in the publications, reports to the government, etc., that are a result of this research.*

ALGEMENE DIRECTIE
Commissie voor Medische Ethiek

VOORZITTER:
Prof dr. P. Deron

SECRETARIS
Prof dr. R. Peleman

INGANG 75
ROUTE 7522

UZ GENT
UNIVERSITEIT GENT

Universitair Ziekenhuis Gent
C. Heymanslaan 10 | B 9000 Gent
www.uzgent.be

* *In the framework of 'Good Clinical Practice', the pharmaceutical company and the authorities have the right to inspect the original data. The investigators have to assure that the privacy of the subjects is respected.*
* *The Ethics Committee stresses that it is the responsibility of the promotor to guarantee the conformity of the non-dutch informed consent forms with the dutch documents.*
* *None of the investigators involved in this study is a member of the Ethics Committee.*
* *All effective members of the Ethics Committee, or their representatieves, have reviewed this project. (The list of the members is enclosed)*

Namens het Ethisch Comité / On behalf of the Ethics Committee

Prof. dr. P. Deron
Voorzitter / Chairman

CC: UZ Gent – HIRUZ CTU
FAGG - Research & Development; Victor Hortaplein 40, postbus 40 1060 Brussel
Prof. dr. Jan Victor

B

Ledenlijst op 17/11/2021

Voorzitter: Prof. dr. P. Deron
Secretaris: Prof. Dr. R. Peleman

Effectief lid	plaatsvervangend lid
Dr. G. VAN LANCKER (UZG – klinisch farmacoloog, ♀)	Prof. Dr. S. ROTTEY (UZG – klinisch farmacoloog, ♀)
Prof.dr. D. DE BACQUER (UG - statisticus, ♂)	Prof. dr. P. COOREVITS (UG - statisticus, ♂)
Dr. J. VAN ELSEN (huisarts, ♂)	Dr. M. COSYNS (huisarts, ♂)
Prof. dr. K. DE GROOTE (UZG – kindercardioloog, ♀)	Prof.dr. P. SCHELSTRAETE (UZG – kinderpneumoloog/infectioloog, ♀)
Prof.dr. W. NOTEBAERT (UG – psycholoog, ♂)	Mr. W. SCHRAUWEN (UZG – psycholoog, ♂)
Mevr. M. FOUQUET (UZG – verpleegkundige, ♀)	Mevr. I. VLERICK (UZG – verpleegkundige, ♀)
Dhr. C. DEMEESTERE (UZG – verpleegkundige, lic. Medisch sociale wetenschappen, ♂)	Dhr. G. DE SMET (UZG – verpleegkundige, - lic. Medisch sociale wetenschappen ♂)
Mevr. K. KINT (UZG – apotheker, ♀)	Mevr. L. HUYS (UZG – apotheker, ♀)
Dhr. B. VANDERHAEGEN (UZG - moraaltheoloog, ♂)	Prof.dr. S. STERCKX (UG - moraalfilosoof, ♀)
Prof.dr. mr. T. BALTHAZAR (UG - jurist, ♂)	Prof. Dr. T. GOFFIN (UG - jurist, ♂)
Mevr. C. VANCAENEGHEM (patiëntvertegenwoordiger, ♀)	Mevr. S. DE GROOTE (patiëntvertegenwoordiger, ♀)
Prof. dr. P. DERON (UZG – chirurg, ♂)	Prof.dr. W. CEELEN (UZG – chirurg, ♂)
Prof. dr. R. PELEMAN (UZG - internist/pneumoloog, ♂)	Prof.dr. H. VERSTRAELEN (UZG – Vulva-arts, ♂)
Prof.dr. J. DECRUYENAERE (UZG – internist/intensivist, ♂)	Dr. N. PETERS (UZG – fertiliteitsarts, ♀)
Prof.dr. R. RUBENS (UZG – internist/endocrinoloog, ♂)	Prof.dr. W. VAN BIESEN (UZG – nefroloog, ♂)
Prof.dr. M. De MUYNCK (UZG – arts fysische geneeskunde en revalidatie, ♀)	Dr. S. JANSSENS (UZG – geneticus, ♀)
Prof. dr. K. DHONDT (UZG – (kinder)psychiater, ♀)	Dr. L. GOOSSENS (UZG – neonatoloog, ♀)

De beoordeling gebeurt door de effectieve leden. Indien een effectief lid niet kan beoordelen, gebeurt de beoordeling door zijn/haar plaatsvervangend lid.

Leden van de commissie die actief betrokken zijn bij een onderzoeksprotocol, werden d'office uitgesloten van beoordeling.

C

Appendix B: Dutch summary

Inleiding: Congruente, wrijvingsarme beweging tussen de articulerende oppervlakken van een synoviaal gewricht is een cruciale voorwaarde voor een duurzame en efficiënte gewrichtsfunctie. Wanneer echter stoornissen optreden in de vorming of het onderhoud (homeostase) van gewrichten, zullen mechanische overbelasting en artrose volgen. Artrose is de meest voorkomende chronische gewrichtsziekte met een wereldwijde prevalentie van 7%. Artrose in de knie vormt 83% van de wereldwijde ziektelast voor artrose. De prevalentie verergert met de tijd en zal naar verwachting blijven oplopen als gevolg van toenemende obesitas en trends van een vergrijzende bevolking. Contra-intuïtief is er weinig bekend over de etiologie en oorzaken van het ontstaan en de progressie van de ziekte. Aangezien het *in vivo* meten van contactkrachten in het kniegewricht een uitdaging blijft, worden computermodellen van het bewegingsapparaat steeds populairder voor niet-invasieve schattingen van de verdeling van de gewrichtsbelasting. Meestal zijn deze methoden afhankelijk van omslachtige en tijdrovende handmatige segmentaties van de gewrichtsgeometrie. Het doel van de huidige studie is het valideren van een geautomatiseerde methode voor gepersonaliseerde distale femorale kraakbeenkartering, ontwikkeld binnen de afdeling orthopedie van het Universitair Ziekenhuis Gent.

Materialen en methoden: In de validatiestudie werden 30 proefpersonen geïncludeerd. Zij voerden een kinetische studie uit en ondergingen magnetische resonantiebeeldvorming van de onderste ledematen. Door manuele segmentatie werd een driedimensionaal beeld van het distale femur, proximale tibia en het rechter distale femurkraakbeen gegenereerd. De gehele femur, nodig voor de kraakbeenkartering, werd gereconstrueerd met behulp van een statistisch vormmodel. De voorspelling van de kraakbeengeometrie door middel van een knooppuntspecifieke diktekaart werd vergeleken met de manuele segmentatie.

Resultaten: De validatiestudie van de geautomatiseerde distale femorale kraakbeen kartering resulteerde in een mediane Root Mean Square Error (RMSE) (0,6723 mm), Average Surface Distance (ASD) (0,5580 mm) en Hausdorff Distance (HD) (2,4165 mm) met de bijbehorende range. Visuele illustratie van locatie specifieke afwijkingen beschrijft de gebieden met de grootste fout.

Discussie: De fout ten opzichte van de lokale kraakbeendikte is een aanvaardbare afwijking. De mediane HD geeft aan dat verdere optimalisatie van de methode gerechtvaardigd is. Ondanks de hoge HD-waarden is de gemiddelde fout relatief laag. Er is dus een grote spreiding in de nauwkeurigheid van de voorspelling bij een proefpersoon. De range van de RMSE, ASD en HD wijst op een grote foutenvariatie tussen de proefpersonen. De belangrijkste voorspellingsfout bevindt zich frontaal, proximaal en bilateraal op de femorale

trochlea, en distaal op de plaats waar het mediale en laterale condylaire kraakbeen samenkomen. Deze fouten zijn niet enkel afkomstig van het voorspellingsmodel.

Conclusie: Een statistisch vormmodel kan anatomische en biomechanische risicofactoren efficiënter opsporen door omslachtige en operator-afhankelijke manuele segmentatie te vervangen. Het schatten van gewrichtskrachten op de knie en de weke delen functie in de knie en het voorspellen van secundaire kinematica van de knie zal mogelijk zijn en patiëntspecifieke gewrichtspreservatie of vervangingsoperatie van de knie zal toepasbaar zijn aan de hand van een voorspellingsmodel. Ondanks dat optimalisatie van het kraakbeenkarteringsmodel verder gerechtvaardigd is, leverde de validatiestudie hoopvolle resultaten op.

Appendix C: Flyer to recruit subjects

Gepersonaliseerde Bewegingsanalyse van het Onderste Lidmaat

Indien u 18 jaar bent of ouder is deze gratis studie misschien iets voor u!

Studie-inhoud

Wij zijn op zoek naar gezonde vrijwillige volwassenen om de relatie tussen de structuur van het menselijk lichaam en beweging in kaart te brengen

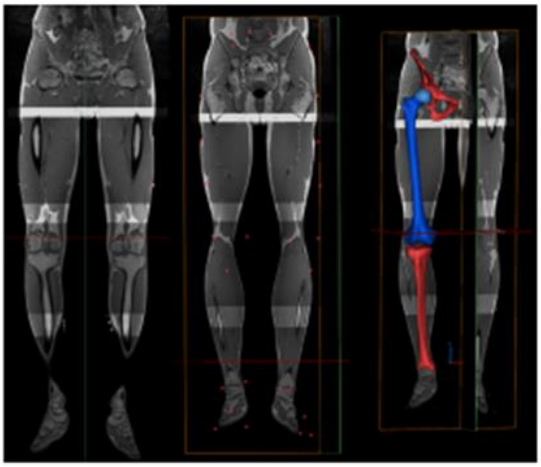

Verloop

- **U komt eenmalig langs op het UZ Gent.**
- **Een ganganalyse en een MRI scan worden afgenomen.**

Wie?

- **U bent tussen de 18 en 50 jaar oud?**
- **U heeft geen gewrichtsproblematiek van het onderste lidmaat?**
- **U onderging geen voorgaande operaties aan heup, knie of enkel?**
- **U hebt geen medische tegenaanwijzingen voor het nemen van een MRI scan?**

Contact

- **Matthias.Peiffer@ugent.be**
- **Aline.Vanoevelen@ugent.be**
- **Kate.Duquesne@ugent.be**

UZ GENT UNIVERSITEIT GENT FACULTEIT GENEESKUNDE EN GEZONDHEIDSWETENSCHAPPEN fwo GIFMI

Appendix D: Informed consent

Informatiebrief voor de deelnemers aan een experiment

Titel van de studie:

Op weg naar gepersonaliseerde kraakbeenpredictie van het onderste lidmaat: Validatie van reactiekrachten en weke delen anatomie ter hoogte van de knie en enkel

Beste,

U wordt uitgenodigd om deel te nemen aan een klinische studie. Neem, voor u beslist deel te nemen aan deze studie, voldoende tijd om deze informatiebrief aandachtig te lezen en dit te bespreken met de onderzoeker of zijn/haar vertegenwoordiger, of met andere mensen. Neem ook de tijd om vragen te stellen indien er onduidelijkheden zijn of indien u bijkomende informatie wenst. Dit proces wordt 'informed consent' of 'geïnformeerde toestemming' genoemd. Eens u beslist heeft om deel te nemen aan de studie zal men u vragen om het toestemmingsformulier achteraan deze bundel te ondertekenen.

1 WAT IS HET DOEL VAN DE STUDIE?

Wij nodigen u uit om deel te nemen aan een klinische studie met als doel een beter inzicht te verkrijgen in de gepersonaliseerde bewegingsanalyse van het onderste lidmaat. Hierbij zal een persoon-specifieke anatomie worden gekoppeld aan het corresponderende gangpatroon. Het doel hierbij is om de invloed van de vorm op de functie van het onderste ledemaat in kaart te brengen.

De opdrachtgever van deze studie is het Universitair Ziekenhuis Gent. Zowel artsen, postdoctorale onderzoekers, doctoraatstudenten, studenten geneeskunde en studenten podologie zullen deel uitmaken van het onderzoeksteam.

2 WAT HOUDT DEELNAME AAN DE STUDIE IN VOOR U?

Deelname houdt 1 bezoek aan het UZ Gent in.

Tijdens het eerste deel van het bezoek zal door middel van een ganganalyse uw bewegingspatroon worden geregistreerd. Tijdens het tweede deel van het bezoek zal een MRI van het onderste lidmaat gemaakt worden. Daardoor kan uw persoonlijke anatomie (=bouw van het lichaam) in beeld gebracht worden.

3 HOEVEEL PERSONEN ZULLEN AAN DEZE STUDIE DEELNEMEN?

Er zullen in totaal 60 personen aan deze studie deelnemen.

4 WAT IS DE DUUR VAN DEZE STUDIE?

De verwachte totale duur van de studie voor u is een halve dag (3 tot 4 uur).

5 WAT WORDT VERWACHT VAN DE DEELNEMER?

Voor het welslagen van de studie, is het uitermate belangrijk dat u volledig meewerkt met de onderzoeker en dat u zijn/haar instructies nauwlettend opvolgt.

Bovendien moet u onderstaande items respecteren:

- U mag niet zwanger zijn
- U heeft geen implantaat of elektrische/mechanische apparatuur/elektrode in het lichaam (bv. pacemaker, pijn/medicatiepomp, vaatclips, shunt, hartkleppen, prothese, gehoorapparaat, …)
- U werd nooit verwond aan de ogen of de huid ten gevolge van metalen splinters (accidenteel na metaalbewerking, shrapnel, kogel, …)
- U draagt geen Permanente makeup
- U onderging nooit een operatie aan het hoofd of hart.
- U heeft geen systeemaandoeningen (zoals bv diabetes, reuma, …) met invloed op uw gangpatroon.
- U mag in het verleden geen voorgaande chirurgie van het onderste lidmaat ondergaan hebben.
- U hebt geen gekende kraakbeenschade van de gewrichten van het onderste lidmaat
- U hebt geen meerdere voorgaande verstuikingen gehad die een blijvende instabiliteit van de enkel veroorzaken
- U hebt geen pijnscore van >3/10 aan een of meerdere gewrichten van het onderste lidmaat
- U kan zelfstandig stappen zonder hulpmiddelen

6 WELKE PROCEDURES VINDEN TIJDENS DE STUDIE PLAATS?

6.1 Procedures:

1. Ganganalyse zal worden uitgevoerd met behulp van de GRAIL® (Motek, Amsterdam, Nederland) geïnstrumenteerde loopband, dewelke in overeenkomst beschikbaar is voor dit onderzoek in het smart space lab (Revalidatiecentrum, K7, UZ Gent). Tijdens het stappen op de loopband worden de bewegingen geregistreerd en de krachten onder de voet gemeten. Om de beweging te registreren zullen reflecterende markers worden aangebracht met hypoallergene (= minder kans op een allergische reactie hierop) kleefband. Er zal blootsvoets gestapt worden.

2. Gepersonaliseerde anatomie (= bouw van het lichaam) zal worden voorzien door middel van MRI scans. Deze beeldvormingstechniek gebruikt sterke magneetvelden en radiogolven om weefsel te onderzoeken. U neemt plaats op een onderzoekstafel in een zaal met een sterk magneetveld. Deze tafel wordt in een tunnelvormig apparaat geschoven, waar voldoende lucht en

ventilatie aanwezig is. De scantijd bedraagt minder dan een halfuur. Hierbij verwerkt een computer de verschillende signaalintensiteiten tot medische beelden.

6.2 Studieverloop:

Indien u besluit deel te nemen aan de studie en aan alle voorwaarden voor deelname voldoet, zal u onderstaande testen en onderzoeken doorlopen:

1. Screeningsfase

Na inclusie in de studie, zullen wij via mail met u een aantal vragen overlopen om de komende onderzoeken op een veilige manier te laten verlopen. Tevens zullen wij met u bekijken wanneer deze onderzoeken kunnen doorgaan, op een moment dat past in uw agenda.

2. Onderzoeksfase (UZ Gent)

2.1. Ganganalyse (Eenmalig, duurtijd circa 2 uur)
2.2. MRI scan (Eenmalig, duurtijd circa 1 uur)

7 WAT ZIJN UW RECHTEN BIJ DEELNAME AAN DEZE STUDIE?

De deelname aan deze studie is volledig vrijwillig, er kan op geen enkele manier sprake zijn van dwang. U kunt weigeren om deel te nemen aan de studie en u kunt zich op elk ogenblik terugtrekken uit de studie zonder dat u hiervoor een reden moet opgeven en zonder dat dit op enige wijze een invloed zal hebben op de verdere relatie met de onderzoeker.

Uw deelname aan deze studie zal beëindigd worden als de onderzoeker meent dat dit in uw belang is. U kan ook voortijdig uit de studie teruggetrokken worden door de onderzoeker als u de in deze informatiebrief beschreven procedures niet goed opvolgt of u de beschreven items niet respecteert.
Indien u uit de studie gehaald wordt, zullen de reeds verzamelde gepseudonimiseerde gegevens in de databank blijven voor analyse, maar er zal geen nieuwe data toegevoegd worden.

Deze studie werd vooraf goedgekeurd door een onafhankelijke Commissie voor Medische Ethiek verbonden aan het Universitair Ziekenhuis van Gent en de Universiteit Gent. De studie wordt uitgevoerd volgens de richtlijnen voor de goede klinische praktijk (ICH/GCP) en de verklaring van Helsinki opgesteld ter bescherming van mensen deelnemend aan klinische studies. In geen geval dient u de goedkeuring door de Commissie voor Medische Ethiek te beschouwen als een aanzet tot deelname aan deze studie.

7.1 Vertrouwelijkheid

In overeenstemming met de Algemene Verordening Gegevensbescherming (of GDPR) (EU) 2016/679 van 27 april 2016 (die vanaf 25 mei 2018 in voege is) en de Belgische wet van 30 juli 2018, betreffende de bescherming van natuurlijke personen in verband met de verwerking van persoonsgegevens en betreffende het vrije verkeer van die gegevens, zal uw persoonlijke levenssfeer worden gerespecteerd en kan u toegang krijgen tot de verzamelde gegevens. Elk onjuist gegeven kan op uw verzoek verbeterd worden.
Uw toestemming om deel te nemen aan de studie betekent dat we gegevens van u verwerken voor het doel van de klinische studie. Deze verwerking van gegevens is wettelijk voorzien op basis van artikel 6, § 1, (a) en artikel 9, § 2(j) van de Algemene Verordening Gegevensbescherming.

Alle informatie die tijdens deze studie verzameld wordt zal gepseudonimiseerd worden (hierbij kan men uw gegevens nog terug koppelen naar uw persoonlijk dossier). In het geval van pseudonimisering zal de sleutel tot deze codes enkel toegankelijk zijn voor de onderzoeker of de door hem/haar aangestelde vervanger. In deze studie kunnen ook algemene gezondheidsgegevens verzameld worden. U zal tevens gevraagd worden een persoonlijk email-adres te bezorgen waarop de onderzoekers u kunnen bereiken voor eventuele verdere vragen. Enkel de gepseudonimiseerde gegevens zullen gebruikt worden voor analyse van de gegevens en in alle documentatie, rapporten of publicaties (in medische tijdschriften of congressen) over de studie. Vertrouwelijkheid van uw gegevens wordt dus steeds gegarandeerd. Zowel persoonlijke gegevens als gegevens aangaande uw gezondheid zullen verwerkt en bewaard worden gedurende minstens 20 jaar. De verwerkingsverantwoordelijke van de gegevens is de instelling van de hoofdonderzoeker van de studie, Prof. Dr. Emmanuel Audenaert (UZ Gent). Zijn onderzoeksteam zal toegang krijgen tot uw persoonsgegevens. In het kader van de gegevensbescherming zullen de gegevens verwerkt worden door personen behorend tot het onderzoeksteam en aangeduid door en onder de verantwoordelijkheid van de hoofdonderzoeker, inclusief interne medewerkers met een niet-gezondheidszorgberoep.

De Data Protection Officer kan u desgewenst meer informatie verschaffen over de bescherming van uw persoonsgegevens. Contactgegevens: Katya Van Driessche, dpo@uzgent.be.

Vertegenwoordigers van de opdrachtgever, auditoren, de Commissie voor Medische Ethiek en de bevoegde overheden, allen gebonden door het beroepsgeheim, hebben rechtstreeks toegang tot uw medische dossiers om de procedures van de studie en/of de gegevens te controleren, zonder de vertrouwelijkheid te schenden. Dit kan enkel binnen de grenzen die door de betreffende wetten zijn toegestaan. Door het toestemmingsformulier, na voorafgaande uitleg, te ondertekenen, stemt u in met deze toegang.

De Belgische toezichthoudende instantie die verantwoordelijk is voor het handhaven van de wetgeving inzake gegevensbescherming is bereikbaar via onderstaande contactgegevens:

Gegevensbeschermingsautoriteit (GBA)
Drukpersstraat 35 – 1000 Brussel
Tel. +32 2 274 48 00
e-mail: contact@apd-gba.be
Website: www.gegevensbeschermingsautoriteit.be

7.2 Verzekering

De opdrachtgever voorziet in een vergoeding en/of medische behandeling in het geval van schade en/of letsel ten gevolge van deelname aan deze klinische studie. Voor dit doeleinde is een verzekering afgesloten met foutloze aansprakelijkheid conform de wet inzake experimenten op de menselijke persoon van 7 mei 2004 (Allianz Global Corporate & Specialty – polisnummer opdrachtgever UZ Gent BEL001889 – polisnummer opdrachtgever UGent BEL000862). Indien de onderzoeker van mening is dat er verband met de studie mogelijk is, zal hij/zij de aangifteprocedure bij de verzekering starten. Op dat ogenblik kunnen uw gegevens doorgegeven worden aan de verzekeraar. In het geval van onenigheid met de onderzoeker of met de door de verzekeringsmaatschappij aangestelde expert, en steeds wanneer u dit nodig acht, kunnen u, of in geval van overlijden uw rechthebbenden, de verzekeraar rechtstreeks in België dagvaarden (Allianz Global Corporate & Specialty; Uitbreidingstraat 86, 2600 Berchem; Tel: +32 33 04 16 00).

8 WAT ZIJN DE RISICO'S EN VERWACHTE VOORDELEN BIJ DEELNAME AAN DEZE STUDIE?

Deelname aan deze studie brengt voor u geen onmiddellijk voordeel. Uw deelname in de studie kan wel helpen om in de toekomst de bewegingspatronen van het onderste lidmaat beter te kunnen begrijpen alsook patiënten met locomotorische problematiek van het onderste lidmaat beter te kunnen helpen.

De *"Grail"* is een veilig en gecertificeerd laboratorium voor klinische bewegingsanalyse. Hierbij meten en analyseren we op een gestandaardiseerde en objectieve wijze uw gangpatroon. Dit bevat geen schadelijke straling voor de patiënt. Theoretisch gezien, zijn de mogelijke risico's: valaccident, gekneld zitten met de voet tussen de loopband en contactallergie op basis van de dubbelzijdige marker tape voor bewegingsregistratie. De medewerkers van deze studie zijn opgeleid om dit instrument te gebruiken en met de nodige voorzorgsmaatregelen is het risico op ongevallen minimaal.

Een MRI-onderzoek gebruikt geen röntgenstralen, is niet pijnlijk en ook niet schadelijk. U kunt wel trillingen of warmte voelen. Dat is normaal en ongevaarlijk. Het toestel is lawaaierig, daarom krijgt u oordoppen en een hoofdtelefoon waarmee u zich moet beschermen. De medewerkers die het toestel bedienen, hebben allen een MRI safety course doorlopen en observeren u permanent. U krijgt ook een bel in de hand waarmee u hen in geval van nood kunt waarschuwen.

U hebt het recht op elk ogenblik vragen te stellen over de mogelijke en/of gekende risico's van deze studie. Als er in het verloop van de studie gegevens aan het licht komen die een invloed zouden kunnen hebben op uw bereidheid om te blijven deelnemen aan deze studie, zult u daarvan op de hoogte worden gebracht. Mocht u door uw deelname aan de studie toch enig nadeel ondervinden, zal u een gepaste behandeling krijgen.

9 ZIJN ER KOSTEN VERBONDEN AAN DE DEELNAME AAN DEZE STUDIE?

Uw deelname aan deze studie brengt geen extra kosten mee voor u.

10 IS EEN VERGOEDING VOORZIEN BIJ DEELNAME AAN DEZE STUDIE?

Er is geen vergoeding voorzien bij deelname aan deze studie.

11 TOT WIE KUNT U ZICH RICHTEN IN HET GEVAL VAN PROBLEMEN OF INDIEN U VRAGEN HEEFT?

Als er een letsel optreedt ten gevolge van de studie, of als u aanvullende informatie wenst over de studie of over uw rechten en plichten, kunt u in de loop van de studie op elk ogenblik contact opnemen met de onderzoeker of een medewerker van zijn of haar team:

Naam: Matthias Peiffer

E-mail: Matthias.Peiffer@UGent.be

Telefoonnummer: +32 9 332 6884

Naam: Aline Van Oevelen

E-mail: Aline.VanOevelen@UGent.be

Naam: Kate Duquesne

E-mail: Kate.Duquesne@UGent.be

Naam: Emmanuel Audenaert

E-mail: Emmanuel.Audenaert@UGent.be

Telefoonnummer: +32 9 332 22 51

L

TOESTEMMINGSFORMULIER VOOR DE DEELNEMERS AAN EEN EXPERIMENT

Referentienummer van de deelnemer voor deze studie	

Ik heb het document "Informatiebrief voor de deelnemers aan een experiment" pagina 1 tot en met 7 gelezen en begrepen en ik heb er een kopij van gekregen. Ik heb uitleg gekregen over de aard, het doel, de duur, de te voorziene effecten van de studie en over wat men van mij verwacht. Ik heb uitleg gekregen over de mogelijke risico's en voordelen van de studie. Men heeft me de gelegenheid en voldoende tijd gegeven om vragen te stellen over de studie en ik heb op al mijn vragen een bevredigend antwoord gekregen, ook op medische vragen.
Ik begrijp dat deelname aan de studie vrijwillig is en dat ik mij op elk ogenblik uit de studie mag terugtrekken zonder een reden voor deze beslissing op te geven en zonder dat dit op enigerlei wijze een invloed zal hebben op de verdere relatie met de onderzoeker.
Ik begrijp dat auditors, vertegenwoordigers van de opdrachtgever, de Commissie voor Medische Ethiek of bevoegde overheden, mijn gegevens mogelijks willen inspecteren om de verzamelde informatie te controleren. Bovendien ben ik op de hoogte dat bepaalde gegevens doorgegeven worden aan de opdrachtgever van de studie. Te allen tijde zal mijn privacy gerespecteerd worden.
Ik ben me ervan bewust dat deze studie werd goedgekeurd door een onafhankelijke Commissie voor Medische Ethiek verbonden aan het UZ Gent en de Universiteit Gent en dat deze studie zal uitgevoerd worden volgens de richtlijnen voor de goede klinische praktijk (ICH/GCP) en de verklaring van Helsinki, opgesteld ter bescherming van mensen deelnemend aan experimenten. Deze goedkeuring was in geen geval de aanzet om te beslissen om deel te nemen aan deze studie.
Men heeft mij ingelicht dat zowel persoonlijke gegevens als gegevens aangaande mijn gezondheid worden verwerkt en bewaard gedurende minstens 20 jaar. Ik ben op de hoogte dat ik recht heb op toegang en op verbetering van deze gegevens. Aangezien deze gegevens verwerkt worden in het kader van medisch-wetenschappelijke doeleinden, begrijp ik dat de toegang tot mijn gegevens kan uitgesteld worden tot na beëindiging van het onderzoek. Indien ik toegang wil tot mijn gegevens, zal ik mij richten tot de onderzoeker die verantwoordelijk is voor de verwerking ervan.

Aankruisen door de deelnemer indien akkoord

Ik stem in om deel te nemen aan de volgende delen van de studie:

1) Ik stem ermee in om volledig samen te werken met de onderzoeker. Ik zal hem/haar op de hoogte brengen als ik onverwachte of ongebruikelijke symptomen ervaar.	
2) Ik ben akkoord dat er een ganganalyse zal worden uitgevoerd	
3) Ik ben akkoord dat er een MRI scan zal worden uitgevoerd	
4) Ik stem ermee in dat mijn email adres gebruikt wordt voor eventueel later contact.	

Naam en voornaam van de deelnemer	Handtekening	Datum
Naam en voornaam van de onderzoeker*	Handtekening	Datum

2 kopieën dienen te worden vervolledigd. Het origineel wordt door de onderzoeker bewaard in het ziekenhuis gedurende 20 jaar, de kopie wordt aan de deelnemer gegeven.

* Aankruisen door de onderzoeker indien akkoord

Ik verklaar de benodigde informatie inzake deze studie (de aard, het doel, en de te voorziene effecten) mondeling te hebben verstrekt evenals een exemplaar van het informatiedocument aan de deelnemer te hebben verstrekt.	
Ik bevestig dat geen enkele druk op de deelnemer is uitgeoefend om hem/haar te doen toestemmen tot deelname aan de studie en ik ben bereid om op alle eventuele bijkomende	

M

vragen te antwoorden.	

Appendix E: Pre-MRI examination questionnaire

SCREENINGSFORMULIER VOOR PROEFPERSONEN VOOR DE MRI PROCEDURE

Ghent Institute for Functional and Metabolic Imaging

GIfMI

Dit document dient door elke proefpersoon die onderzocht wordt met de MRI-faciliteiten van het GIfMI te worden ingevuld. Het document is geldig voor de duur van één scansessie. De verstrekte informatie valt onder het beroepsgeheim.

NAAM ONDERZOEKER:	
DATUM:	STUDIENR:

NAAM PROEFPERSOON:	TEL.
GEWICHT EN LENGTE: KG - CM	GEBOORTEDATUM:

⚠ MRI maakt gebruik van een **sterk magnetisch veld dat altijd aan staat.** Elk voorwerp dat in de MRI-zaal wordt gebracht betekent een potentieel gevaar. Mogen wij u vriendelijk verzoeken ...

- ... deze lijst waarheidsgetrouw en volledig in te vullen.
- ... steeds de instructies van de onderzoeker op te volgen.
- ... voorwerpen met metalen onderdelen te verwijderen (gehoorapparaat, kunstgebit, bril, haarspeld, gsm, horloge, sleutels, portefeuille, munten, paperclips, balpennen, aansteker, ...) en uw kledingzakken leeg te maken.

	JA	NEEN
Onderging u ooit een operatie aan het hoofd of hart? Zo ja, dateer en beschrijf de ingreep.	☐	☐
Heeft u enig implantaat of elektrische/mechanische apparatuur/elektrode in het lichaam (bv. pacemaker, pijn/medicatiepomp, vaatclips, shunt, hartkleppen, prothese, gehoorapparaat, ...)? Tandvullingen zijn géén contra-indicatie. Zo ja, dateer en beschrijf:	☐	☐
Werd u ooit verwond aan de ogen of de huid ten gevolge van metalen splinters (accidenteel na metaalbewerking, shrapnel, kogel, ...)?	☐	☐
Heeft u momenteel koorts?	☐	☐
Voor de vrouwelijke proefpersonen: bent u (mogelijks) zwanger?	☐	☐

O

Indien u nog mogelijks relevante informatie heeft die bovenstaand niet aan bod kwam, kunt u dit hier melden:

.....

.....

.....

Opmerkingen vanwege de onderzoeker:

.....

.....

.....

Verklaring bestemd voor de proefpersoon:

"Ik verklaar naar best vermogen dat de bovenstaande informatie correct en volledig is. Ik heb de volledige inhoud van dit formulier gelezen en begrepen en heb de mogelijkheid gehad om vragen te stellen betreffende de informatie op dit formulier.

Handtekening en datum:

Verklaring bestemd voor de onderzoeker:

"Ik verklaar de proefpersoon volledig geïnformeerd te hebben over de gevraagde informatie op dit formulier met voldoende vrijheid tot vraagstelling."

Handtekening en datum:

Appendix F: Post-MRI examination questionnaire

CONTROLEFORMULIER VOOR PROEFPERSONEN NA DE MRI PROCEDURE

Ghent Institute for Functional and Metabolic Imaging

GIFMI

Verantwoordelijke onderzoeker:	
Datum:	Studienaam/nr deelnemer:
Scantijd:	Sequenties: ☐ MPRAGE ☐fMRI ☐ DTI ☐ ASL ☐ Andere: .....

Naam deelnemer:
Geboortedatum:

⚠ Dit is een checklist die specifiek vraagt naar zeldzame maar mogelijke neveneffecten ten gevolge het gebruik van MRI.

Heeft u een van de volgende effecten gevoeld?	**JA**	**NEEN**	**COMMENTAAR**
Claustrofobie?	☐	☐	
Duizeligheid?	☐	☐	
Misselijkheid?	☐	☐	
Warmte?	☐	☐	
Koude?	☐	☐	
Metaalsmaak?	☐	☐	
Hoofdpijn?	☐	☐	
Onwillekeurige spiercontracties?	☐	☐	
Andere			

Verklaring bestemd voor de proefpersoon: ***"Ik verklaar dat deze informatie correct en volledig is."***

Handtekening deelnemer:

Handtekening onderzoeker:

Q

Appendix G: Segmentation settings

1. The setting of the masks

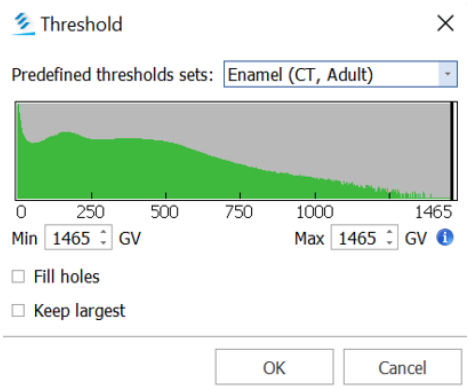

2. The settings of the multiple-slice edit

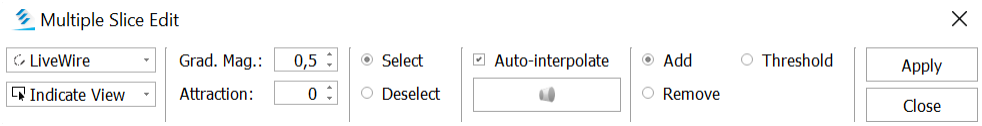

3. The settings of the region grow

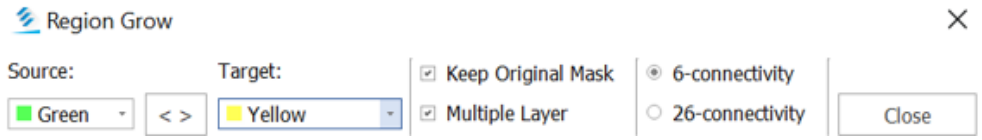

4. The settings of the smooth